Consequences of NMDA receptor deficiency can be rescued in the adult brain

Catharine A. Mielnik[1], Yuxiao Chen[1*], Mary A. Binko[2*], Rehnuma Islam[2], Marija Milenkovic[1], Wendy Horsfall[1], Ali Salahpour[1], Evelyn K. Lambe[2], and Amy J. Ramsey[1,2]

[1] Department of Pharmacology & Toxicology, [2] Department of Physiology, University of Toronto, Toronto, ON, M5S 1A8, Canada

Amy Ramsey
1 King's College Circle
Room 4302 Medical Sciences Building
Toronto, ON M5S 1A8 Canada
(416) 978-2509
a.ramsey@utoronto.ca

Highlights:

GluN1 inducible rescue mice allow recovery of functional NMDA receptors in a neurodevelopmental model of schizophrenia.

Rescue in adolescent or adult mice achieves a similar level of functional recovery.

Cortically-mediated behaviors show complete or near complete rescue, but subcortically-mediated behaviors show limited rescue.

Higher-order brain function appears amenable to treatment in adulthood and surprisingly unencumbered by critical period.

SUMMARY

NMDA receptors (NMDAR) are important in the formation of activity-dependent connections in the brain. In sensory pathways, NMDAR disruption during discrete developmental periods has enduring effects on wiring and function. Yet, it is not clear whether NMDAR-limited critical periods exist for higher-order circuits governing mood and cognition. This question is urgent for neurodevelopmental disorders, like schizophrenia, that have NMDAR hypofunction and treatment-resistant cognitive symptoms. As proof of concept, we developed a novel mouse model where developmental NMDAR deficits can be ameliorated by inducible Cre recombinase. Rescue of NMDARs in either adolescence or adulthood yields surprisingly strong improvements in higher-order behavior. Similar levels of behavioral plasticity are observed regardless of intervention age, with degree of plasticity dependent on the specific behavioral circuit. These results reveal higher-order brain function as amenable to treatment in adulthood and identify NMDAR as a key target for cognitive dysfunction.

INTRODUCTION

Neuroplasticity refers to the malleable nature of brain cells to change their physiology and connectivity with experience, and it is fundamental to the cellular events that mediate brain development, learning, memory, and repair (Sale et al., 2014). Conventionally the juvenile brain is described as being more plastic than the adult brain,

which has well-established patterns of connectivity (Ehninger et al., 2008). This concept has been termed ‘young age plasticity privilege’ (Dennis et al., 2013). An explanation for the increased plasticity of the developing brain is that NMDA-type glutamate receptors contain GluN2B subunits in the juvenile brain and GluN2A subunits in the adult brain. The developmental presence of the GluN2B subunit allows for longer open channel times and a greater window for coincidence detection (Tang et al., 1999) enabling activity-dependent Hebbian synapse formation.

During development there are also discrete periods of heightened plasticity termed “critical periods”. Critical periods are time points when specific experiences and neuron activity influence neurogenesis, connectivity, and learning (Hubel and Wiesel, 1963). These critical periods are not only times of heightened plasticity, but they are also times of heightened vulnerability. Perturbations in neuron activity during this time have enduring detrimental consequences. At the molecular level, heightened plasticity is conferred by the enhanced activity of NMDARs (Crair and Malenka, 1995; Tsumoto et al., 1987). The developmental switch from GluN2B- to GluN2A-containing NMDARs may be an underlying mechanism for the closure of key critical periods (Tang et al., 1999). In visual and somatosensory systems, inactivation of NMDARs during the critical period disrupts proper patterns of connectivity (Cline et al., 1987; Goodman and Shatz, 1993; Li et al., 1994; Miller et al., 1989). Thus, disruptions in NMDAR signalling during development can have lasting effects on neuronal patterns of connectivity.

Critical periods in development are most evident in sensory pathways with somatotopic organization. However, it is possible that critical periods also exist for higher-order cognitive systems, potentially delayed in later-maturing regions such as prefrontal cortex (Gogtay et al., 2004; Shaw et al., 2008). As such, impaired NMDAR function during early and adolescent development may have lasting effects on the integrity of cognitive circuits. Indeed, de novo missense mutations in the GluN1 gene have been identified in patients with intellectual disability and schizophrenia (Chen et al., 2017; Tarabeux et al., 2011; Yuan et al., 2015). Beyond this, the role of NMDARs in schizophrenia is strongly supported by GWAS, post-mortem, and PET imaging studies (Hardingham and Do, 2016; Schizophrenia Working Group of the Psychiatric Genomics Consortium, 2014).

Schizophrenia presents a challenge for treatment because diagnosis and intervention take place in adulthood, years after any developmental insult occurs (van Os and Kapur, 2009). Interventions at this late stage may be unable to reverse developmental pathologies. Indeed, antipsychotics fail to treat cognitive symptoms, and it is possible that this failure is due in part to the timing of interventions. To improve the treatment of schizophrenia and other disorders, it is important to determine whether there are critical periods in development for cognition as there are for sensory systems.

Since NMDARs play a central role in activity-dependent connectivity, and are implicated in schizophrenia, we asked whether the developmental consequences of NMDAR hypofunction could be overcome in the mature brain. To address this question, we

developed a new mouse line based on the original GluN1 knockdown mouse (Mohn et al., 1999). The new mice have a global reduction in NMDARs due to an insertion mutation in the *Grin1* gene, and differ from the original line in that the mutation can be excised in a Cre recombinase-dependent manner. We used a tamoxifen-inducible Cre to globally restore NMDARs and investigate the level of phenotypic rescue that can be achieved at different stages of development.

NMDAR function was restored at two postnatal time points, in adolescence and adulthood. These times were chosen to study the plasticity of the brain during and after puberty, which is relevant for the symptom onset of schizophrenia. Another reason to rescue NMDA receptors in adolescence is to target an important time of refinement and maturation in the prefrontal cortex (Shaw et al., 2008). We quantified several behavioral outputs as measures of plasticity, and compared the extent of functional recovery that was achieved with adolescent and adult intervention. We ascertained that behavioral plasticity and phenotypic improvements were the same regardless of intervention time or length of recovery. Strikingly, we discovered that plasticity at the cellular and behavioral level was more evident in the cortex than in the striatum. This study suggests that plasticity of cognitive circuits extends well into adulthood, and that there are regional differences in the ability to upregulate NMDAR activity and to normalize behavioral outputs.

RESULTS

Inducible rescue of NMDAR deficiency

We developed the GluN1-inducible rescue mouse based on the original GluN1 knockdown mouse (Mohn et al., 1999), which has been a key model to better understand the consequences of NMDAR deficiency (Duncan et al., 2004; Dzirasa et al., 2009; Ferris et al., 2014; Gandal et al., 2012; Grannan et al., 2016; Halene et al., 2009; Mielnik et al., 2014; Milenkovic et al., 2014; Moy et al., 2012; 2006). GluN1 inducible-rescue mice (*Grin1*$^{flneo/flneo}$) were developed so that the hypomorphic insertion mutation could be excised, restoring NMDARs in a tightly-regulated temporal fashion.

To generate the *Grin1*$^{flneo/flneo}$ mouse line, a floxed neomycin cassette was inserted into intron 19 of the *Grin1* gene at the same position as the original GluN1 knockdown mutation (Mohn et al., 1999) (Figure 1A). We used a tamoxifen-inducible Cre recombinase to restore the *Grin1* locus globally at specific stages of postnatal development (*ROSA26*^{CreERT2}). To verify Cre induction, a Cre recombinase reporter line (*ROSA26*^{tdTomato}) was used to confirm that the tamoxifen regimen robustly induced global Cre activity (Figure 1, Table S1 and STARmethods). As seen in Figure 1B, in the absence of tamoxifen, there is no expression of tdTomato in the cortex, striatum, hippocampus or cerebellum. Following administration of tamoxifen, there is robust expression of tdTomato in all brain regions, indicating global expression and induction of Cre recombinase with the regimen of tamoxifen.

After treating mice with tamoxifen, we found that GluN1 knockdown mice (*Grin1*$^{flneo/flneo}$) express barely detectable levels of GluN1 protein, and GluN1Cre rescue mice (*Grin1*$^{flneo/flneo}$ x *ROSA26*^{CreERT2}) show a significant increase in GluN1 protein (Figure 1C). Thus the new model has a similar level of GluN1 knockdown to our previously published model, and the added *loxP* sites allow recovery of GluN1 protein. However, recovery of GluN1 protein was roughly half that of wildtype levels, indicating that there are molecular mechanisms engaged that prevented full protein recovery. Since Cre activity was robustly induced throughout the brain (Figure 1B), the incomplete recovery of GluN1 was not due to inadequate Cre activation.

We timed the induction of Cre at 6-and 10-weeks of age to compare the plasticity of the peri-adolescent mouse brain with the mature, adult brain (Figure 1D). Cre induction was achieved by tamoxifen, which is reported to impair cognition (Vogt et al., 2008). For this reason, all genotypes of mice were treated with tamoxifen (WT, WTCre, GluN1, and GluN1Cre). Mice were allowed to recover to 14- or 18-weeks of age to compare mice tested in behavioral assays at the same age and to compare mice given the same recovery time after tamoxifen treatment (Figure 1E). The treatment groups were as follows: Adolescent +8WR (8-weeks recovery), Adult +4WR (4-weeks recovery), and Adult +8WR (8-weeks recovery). All four genotypes were tamoxifen-treated and tested in subsequent behavioral assays and *ex vivo* experiments.

We tested all mice for locomotor activity and stereotypic behavior on the first day of behavioral assessment. This behavioral test was performed on all mice as a treatment

control to ensure comparable levels of rescue were attained within each treatment group. Mice were then assigned to one of two groups for subsequent behavioral tests that spanned three days. (Figure 1E). We verified that the ROSACre transgene did not impact behavior by confirming that the WTCre mice behave similarly to their WT littermates (Figure S1). We also designed the study with sufficient group sizes to determine whether sex affected behavioral outcomes. For the majority of behavioral outcomes, there was no effect of sex. In the instances where there was a statistical effect of sex, or sex by genotype interaction, we observed that the trend for each sex was the same as the grouped data. Overall, sex did not affect the extent of behavioral or biochemical rescue. Figure S2 demonstrates the behavioral outcomes of male and female mice analyzed separately.

Regional variability in the rescue of NMDAR levels

Western blot analysis of GluN1 subunit levels suggested an incomplete recovery of GluN1. However, western blot does not reflect the level of functional NMDARs. NMDARs are composed of two GluN1 subunits and two GluN2 or GluN3 subunits (Traynelis et al., 2010). Normally the GluN1 subunit is not the limiting factor for receptor assembly, and is expressed in excess of GluN2 subunits (Huh and Wenthold, 1999). Therefore, even a partial recovery of GluN1 subunit could translate into a near complete recovery of functional receptors. To quantify receptor levels, we performed radioligand binding with [^{3}H]MK-801. MK-801 binding requires a fully assembled NMDAR tetramer of GluN1 and GluN2 subunits (Kovacic and Somanathan, 2010).

While we had confirmed that our tamoxifen regimen induced global Cre activation, we also considered the possibility that different cells or brain regions vary in their ability to substantially upregulate NMDARs. For this reason, NMDAR levels were measured in membrane preparations (see STARMethods) from four brain regions: cortex, striatum, hippocampus and cerebellum. We used balanced numbers of both sexes, and measured NMDAR levels for all three regimens of intervention and recovery. For each of the three regimens, we verified that MK-801 binding was not affected by the presence of the Cre transgene. (WT vs. WTCre; Table S2).

NMDAR receptor binding densities in WT mice reflect the expected regional differences, where high levels of NMDARs are detected in the hippocampus and cortex, and lower receptor densities are detected in the striatum and cerebellum (Magnusson, 1995). Receptor binding is markedly decreased in all brain regions of GluN1 knockdown mice (Table 1). In the hippocampus and cortex, GluN1 knockdown mice have 12% and 23% of WT NMDAR levels. Receptor levels in the striatum and cerebellum average 30% and 34% of WT respectively. The fold decrease in receptor levels varies between brain regions, but is consistent between intervention groups and ages (Table 1).

Importantly, NMDAR levels are significantly increased in GluN1Cre rescue mice. Receptor levels increase to approximately 50% of wildtype levels in each of the four brain regions that we studied (Table 1). Depending on the timing of intervention and recovery, NMDAR levels in GluN1Cre rescue mice are restored to 56-64% of WT in the

cortex, 48-49% of WT in the hippocampus, 41-50% of WT in the striatum, and 49-59% of WT in the cerebellum.

In summary, the rescue of NMDAR levels, across all intervention time points and all brain regions, is consistently intermediate in nature and plateaus at 50-60% of WT levels. This suggests that the plasticity of NMDAR signaling is intrinsically limited in both the adolescent and adult brain, and that molecular mechanisms prevent 100% recovery of receptor levels.

Reversal of cognitive impairments with adult intervention

Developmental disruption of NMDAR signaling in mice causes behavioral abnormalities that are considered endophenotypes of schizophrenia, autism, and intellectual disability (Gandal et al., 2012; Mielnik et al., 2014; Milenkovic et al., 2014; Mohn et al., 1999; O'Connor et al., 2014; Snyder and Gao, 2013; Uzunova et al., 2014; Wesseling et al., 2014; Zorumski and Izumi, 2012). To determine whether these phenotypes could be rescued with adult intervention, we first studied executive function and social interaction, behaviors that are resistant to treatment with antipsychotics.

Executive function was assessed with the puzzle box test (Ben Abdallah et al., 2011). This paradigm measures the amount of time required for the mouse to reach a goal box by solving different puzzles. The first puzzle for the mouse is reaching the goal box by using an underpass beneath a wall. The second puzzle is digging through bedding in the underpass. The task measures short-term memory by retesting performance two

minutes after the first exposure, and it measures long-term memory by testing performance 24 hours later. Our previous studies indicated that GluN1 knockdown mice perform poorly in all trials of this task, with deficits evident in juvenile mice that become more severe in adult mice (Milenkovic et al., 2014).

As expected, GluN1 knockdown mice take a longer amount of time to reach the goal in all trials, and often fail to reach the goal before the 5-minute cut-off (Figure 2A). However, GluN1Cre rescue show a substantial improvement in executive function by completing the task significantly faster than GluN1 knockdown mice (Figure 2A). Although we hypothesized that adolescent intervention would lead to a more complete recovery that adult intervention, this was not the case. Adult intervention (Adult +8WR) had the best outcome, and intervention at adolescence resulted in the poorest recovery of executive function (Figure 2A).

There was an effect of sex in this task, where WT females reached the goal sooner than WT males (Figure S2E-G). Also, female GluN1Cre rescue mice have a more complete normalization of behavior than male counterparts in the Adult +8WR cohort (Figure S2G). The near-complete rescue of GluN1Cre females at this time point explains why the Adult +8WR group shows the best recovery of executive function (Figure 2A).

We next studied sociability in mice as a measure of social cognition. The sociability test has been used in mice to model social withdrawal symptoms of schizophrenia (Crawley, 2004; Duncan et al., 2004), which are refractory to treatment with most antipsychotics.

We previously determined that GluN1 knockdown mice have adult-onset deficits in social approach behavior, and have reduced activation of cingulate cortex neurons in response to social stimuli (Mielnik et al., 2014; Milenkovic et al., 2014).

While GluN1 mice spend significantly less time in social affiliative behavior, GluN1Cre mice and WT mice investigate a novel mouse for a similar length of time (Figure 2B). This level of rescue is observed regardless of the age at intervention, or the recovery period. In addition, GluN1Cre mice have less erratic exploration patterns than GluN1 mice, and are more focused on the investigation of the novel mouse (Figure 2B). This result suggests that social affiliative behavior is highly plastic in nature, and is amenable to improvement even in adulthood.

Partial improvement in behaviors that engage subcortical limbic structures

GluN1 knockdown mice display a remarkable lack of anxiety in open field tests and in elevated maze tests, with mutant mice preferring to spend more time in the open arms of an elevated maze (Halene et al., 2009). This behavior is also observed in several mouse models of bipolar disorder, and increased time in the open arm is thought to model the fearlessness that occurs in manic episodes (Kirshenbaum et al., 2011; Roybal et al., 2007). We asked whether the mania-like, non-anxious phenotype of GluN1 knockdown mice could be reversed with adult or adolescent rescue of NMDAR deficiency.

Mania-like behavior was measured by the percentage of time spent exploring open arms and closed arms, where more time spent in the open arms compared to closed arms is indicative of decreased anxiety (Lister, 1987). While WT mice spent 10-20% of the time in the open arms, GluN1 knockdown mice had the opposite phenotype and spent almost 100% of the time in the open arms (Figure 2C). The GluN1Cre rescue mice had an intermediate phenotype and spent equal time in the open and closed arms. This effect was observed across all intervention time points (Figure 2C). Thus, in contrast to the near complete rescue of cognitive behaviors, there was only partial rescue of mania-like behavior in the elevated plus maze. Importantly, there was no difference in the degree of behavioral plasticity between the three intervention groups.

Differential recovery of cortical and subcortical-mediated behaviors

Antipsychotics are generally not effective at treating cognitive symptoms in patients, or improving cognitive behaviors in mouse models. However, these drugs do improve positive symptoms in patients, and a drug's antipsychotic efficacy can be predicted in mouse models by their ability to attenuate motor activity and normalize sensorimotor gating (Duncan et al., 2006; Mohn et al., 1999). Locomotor activity and pre-pulse inhibition of acoustic startle response engage both cortical and subcortical structures including the corticostriatal pathway. Antipsychotics are thought to act on medium spiny neurons of the striatum to mediate their therapeutic effects (Li et al., 2016).

Pre-pulse inhibition (PPI) of the acoustic startle response was used to assess sensory processing and the integrity of cortical and subcortical circuits (see STARMethods). The

startle response is an unconditioned and reflexive response to a loud noise, and PPI is the biological phenomenon where a quiet prestimulus noise (prepulse) can suppress that startle response (Paylor and Crawley, 1997).

Several studies reported that the original GluN1 knockdown mutant has deficits in PPI (Islam et al., 2017) that are improved with antipsychotic drugs (Duncan et al., 2006). Consistent with this, GluN1 mice in our study showed a deficit in PPI that was most evident at the lowest prepulse intensities (Figure 3A). Rescue of NMDARs in GluN1Cre mice normalized prepulse inhibition of startle to WT levels. This was observed across all pre-pulse levels and intervention treatment groups (Figure 3A).

Although PPI was fully restored in GluN1Cre mice, the amplitude of the acoustic startle response itself was not rescued (Figure 3A). Both GluN1 and GluN1Cre mice had exaggerated startle responses and the two genotypes were not significantly different from each other (Figure 3A). We noted that cortical and subcortical structures may have different levels of recovery, since the circuitry that mediates the startle response is subcortical, whereas PPI is mediated by distinct circuits involving the thalamus, cortex, and basal ganglia (Swerdlow et al., 2001).

These data suggest that the circuitry underlying PPI is highly plastic in nature, and that adult rescue of NMDARs is sufficient to normalize this aspect of sensory processing. However, the subcortical reflex startle response is generally not plastic, and is not substantially improved at any intervention time point.

Because there was a different level of recovery in cortical and subcortical aspects of the PPI paradigm, we considered this distinction in our analysis of locomotor activity and stereotypy. Locomotor activity and stereotypy engage corticostriatal circuits and are influenced by dopaminergic signalling (Gainetdinov et al., 2001; Lerner and Kreitzer, 2011; Monteiro and Feng, 2016; Welch et al., 2007). Placing the animal in a novel environment increases dopamine firing rate, and elevated dopamine increases motor activity and stereotypy (Giros et al., 1996; Li et al., 2003; Mikell et al., 2014). Thus these behaviors are used as measures of dopamine tone and the integrity of corticostriatal circuits.

Both adolescent and adult rescue of NMDARs led to a partial improvement in hyperactivity of GluN1Cre rescue mice (Figure 3B). Interestingly, we observed that GluN1Cre rescue mice habituated to the novel environment, whereas GluN1 knockdown mice did not. The process of habituation engages additional cortical and hippocampal circuits (Bolivar et al., 2000; Leussis and Bolivar, 2006), and rescue of habituation behavior in GluN1Cre mice is consistent with other cognitive improvements. Regardless of their age at intervention or the length of recovery, GluN1Cre mice have a complete normalization of habituation and a partial normalization of hyperactivity (Figure 3B).

Stereotypy was more resistant to rescue in adult mice, and was only modestly improved following recovery of NMDAR levels. GluN1Cre rescue mice showed a decrease in

repetitive movements, but their behaviour was still more similar to that of GluN1 knockdown mice than to WT (Figure 3C). Importantly, the moderate improvements in stereotypy were equivalent across all intervention time points, indicating similar levels of plasticity in adolescence and adulthood.

NMDAR currents are restored in prefrontal cortical neurons

Behavioral and biochemical analysis of the three genotypes showed that changes in the NMDAR signaling system did not depend on intervention time point (adolescence vs. adulthood) or recovery time (4-weeks vs. 8-weeks). Therefore, we performed whole cell recording slice electrophysiology experiments from mice that were treated at 10-weeks of age and allowed to recover for 4-weeks (Adult +4WR). This time frame allowed us to assess the more immediate changes that occur in neuron physiology. We examined the electrophysiological properties of neurons from the cortex and the striatum since we observed differences in the extent of recovery for cortically and subcortically-mediated behaviors.

Layer 5 pyramidal neurons were recorded in medial prefrontal cortex from WT, GluN1 knockdown, and GluN1Cre rescue mice (Figure 4A). Functional NMDARs were probed with bath application of NMDA (30 µM; 60 s). Across the genotypes, there was a significant difference in the NMDAR currents in the prefrontal cortex (Figure 4B). NMDA elicited a prominent inward current in WT mice, with significant attenuation in GluN1 knockdown mice (Figure 4C). In GluN1Cre rescue mice, the NMDAR currents are

greatly increased compared to knockdown (Figure 4C). Across genotypes, the NMDA-elicited currents were blocked by the NMDAR antagonist, APV.

The differences in functional NMDARs occurred in the presence of largely similar intrinsic membrane properties (Table S3). However, capacitance was significantly larger in prefrontal neurons of GluN1Cre rescue compared to WT mice (Figure 4D). Accordingly, we analyzed the current density of the NMDA-elicited currents (Figure 4E) and found that GluN1Cre mice also had greatly increased current density compared to GluN1 mice.

To summarize, GluN1 knockdown decreased functional NMDARs in layer 5 neurons of prefrontal cortex, which were substantially restored by adult rescue of the GluN1 subunit.

No rescue of NMDAR currents in striatal neurons

Since striatum-associated behaviors like stereotypy were only modestly improved in GluN1Cre rescue mice, we also characterized NMDAR currents in the medium spiny neurons of the dorsal striatum (Figure 4F). Across genotypes there was a significant difference in the NMDAR currents (Figure 4G), with currents greatly attenuated in the GluN1 knockdown mice compared to WT (Figure 4H). However, in contrast to the prefrontal cortex, the currents in the dorsal striatum were not restored in the GluN1Cre rescue mice. Thus, adult rescue of the GluN1 subunit did not increase functional NMDARs in the dorsal striatum. Across all genotypes, NMDAR currents were blocked by APV. The intrinsic membrane properties were largely similar across the genotypes (Table S2).

In sum, the electrophysiology data indicate a region-specific restoration of NMDAR function in the adult rescue mice, with substantial recovery of NMDAR currents in the prefrontal cortex but not in the dorsal striatum.

RNAseq identifies the molecular signatures of NMDAR deficiency and recovery

We next explored the molecular signature of the NMDAR hypofunctional state and the changes that occur as the brain recovers from a state of NMDAR deficiency. We selected cerebral cortex for this investigation of gene expression because this region is strongly relevant to the behavioral improvements. Furthermore, both the radioligand binding and electrophysiology showed strong functional recovery in the cortex. Accordingly, RNAseq analysis was performed on cortex samples from WT, GluN1, and GluN1Cre mice. Male mice were used since no effect of sex was seen in radioligand binding and electrophysiology.

Cortical transcript levels were compared between WT and GluN1 knockdown mice to identify those that were significantly altered by NMDAR deficiency (see STARmethods). Over four hundred genes were differentially-expressed in WT and GluN1 knockdown mice (Table S4). These genes were assigned to one of four categories based on whether transcript levels were normalized in GluN1Cre rescue mice (Figure 5A, Table S4). The vast majority of the genes that were altered in the GluN1 knockdown mice were restored either partially (70%) or fully (12%) to WT levels of expression in GluN1Cre rescue mice. A portion (18%) were resistant to rescue and remained at GluN1 knockdown levels. Finally, there were 68 genes that were not differentially

expressed between WT and GluN1 knockdown mice, but were uniquely altered in GluN1Cre mice (Figure 5A, Table S4).

We then performed gene set analysis (over-representation) with ConsensusPathDB (Kamburov et al., 2011) to understand the biological processes that were responsive or resistant to rescue. Genes that were responsive to rescue by NMDAR restoration were over-represented in the processes of trans-synaptic signalling, cation transport, response to corticosteroids, and neurogenesis (Table 2). Genes that were resistant to rescue were over-represented in the processes of trans-synaptic signalling, regulation of adenylate cyclase activity, and neurogenesis (Table 2). There were several pathways that were over-represented in both gene sets, including trans-synaptic signalling and neurogenesis. Figure 5B depicts the set of neurogenesis genes that are rescued, or are resistant to rescue, in the brains of GluN1Cre mice.

As an alternate approach to understanding patterns of gene expression, we also studied those genes with the greatest fold-change as a result of GluN1 knockdown (Figure 5C). These genes had a two-fold or greater change in expression between WT and GluN1 knockdown mice. All but one of these genes normalized toward WT levels in the GluN1Cre rescue mice (Figure 5C).

Fold-change analysis highlighted astrocytic gene expression changes in GluN1 mice, including the upregulation of aggrecan (*Acan*) (Domowicz et al., 2008), and aquaporin1 (*Aqp1*), which is a marker of reactive astrocytes (McCoy and Sontheimer, 2010). Two

astrocytic genes that promote oligodendrocyte differentiation are downregulated in GluN1 mice: myocilin (*Myoc*) (Kwon et al., 2014), and neurotrophin-3 (*Ntf3*) (Barres et al., 1994; Condorelli et al., 1995). Also notable is the altered expression of several genes that participate in Wnt or BMP signalling, including secreted inhibitory factors (*Grem1*, *Fst*, and *Shisa3*) (Gazzerro et al., 2007; Han et al., 2014; Lüdtke et al., 2016), receptors (*Gpr50*, *Lgr5*, and *Lgr6*) (de Lau et al., 2014; Ma et al., 2015; Nakashima et al., 2016), and transcription factors (*Sp7*, *Foxd3*, and *Tfap2c*) (Stewart et al., 2014; Wang et al., 2011). Wnt and BMP signaling regulate astrocyte and neuron fate commitment (Zhang et al., 2015), further highlighting a potential change in GluN1 knockdown adult neurogenesis or trophic support that is normalized in GluN1Cre rescue mice.

Taken together, the RNA-Seq data show that adult rescue of GluN1 largely restores cortical molecular expression. These results show unexpected plasticity in the mature cortex and, together with the restoration of cortical NMDA electrophysiological responses, give mechanistic insight into the observed recovery of higher-order behaviours.

DISCUSSION

We undertook this study to determine whether insults to NMDAR signaling could be overcome by adult rescue and whether there are critical periods in development for higher-order circuits. This question is central to understanding treatment of cognitive symptoms in schizophrenia, which involve both NMDA receptor dysfunction and late intervention. In humans, schizophrenia symptoms emerge after adolescence and are treated in adulthood. We timed our intervention in mice at 6-weeks of age, because this corresponds to puberty in mice and is a period of synapse refinement in the cortex (Sisk and Zehr, 2005). It also corresponds to the developmental stage in humans where prodromal symptoms become evident (van Os and Kapur, 2009). We hypothesized that intervention at adolescence would be more effective to reverse behavioral impairments than later intervention in adult mice, at 10-weeks of age. However, our study completely disproved this hypothesis. Overall, adolescent intervention was equivalent to adult intervention for the behaviors that we studied.

The strategy to achieve temporal rescue of NMDARs takes advantage of a tamoxifen-inducible Cre recombinase (Ventura et al., 2007). Our study design allowed us to treat all groups of mice with tamoxifen. This was done to reduce the likelihood that the behavioural recovery of GluN1Cre mice would be obscured by the drug treatment. However, the behavioral and biochemical measures were remarkably similar with a 2- or 6-week washout, suggesting that tamoxifen had no effect on our measures of recovery. We identified a tamoxifen regimen that induced robust Cre activation

throughout the brain, which was evidenced by dTomato expression in the Cre reporter line. Despite the evidence of widespread Cre activity, there was not full recovery of GluN1 protein. This indicates that one of the limitations to plasticity and functional recovery is the status of the molecular machinery that regulates GluN1 subunit levels.

Importantly, the modest increase in GluN1 subunit translated into substantial rescue at the biochemical and behavioral level. Indeed, there were regional differences in the amount of functional NMDAR that could be restored. While cortex and hippocampus showed high levels of functional NMDARs, the striatum and cerebellum showed only modest increases. This was true at the cellular level as well, where pyramidal neurons in the cortex showed a near complete recovery of NMDA-elicited current, but medium spiny neurons of the striatum showed no improvement.

The explanation for these regional differences in recovery may lie in the intrinsic ability of neurons to adapt to changes in NMDAR activity. GluN1 mice develop in a state of NMDAR hypofunction, and there are likely a number of compensatory adaptations that enable cells and circuits to function despite the impairments to this key neurotransmitter system. The hippocampus and cortex normally express the highest levels of NMDARs (Magnusson, 1995), and this feature may also allow them to upregulate NMDARs without triggering excitotoxicity or seizures.

Regional differences in NMDAR upregulation may also explain why some behaviors were substantially or even fully normalized, while others were only partially improved by

adult rescue. It is difficult to assign complex behaviors to discrete brain regions, but with this caveat in mind we observed that more cortically-driven behaviors were substantially improved, while those behaviors that are largely subcortical were not. For example, performance on the puzzle box task, which relies heavily on cortical and hippocampal structures (Ben Abdallah et al., 2011), was substantially improved. Sociability, which engages the cingulate cortex (Mielnik et al., 2014), was completely rescued. However, the auditory reflex startle was not rescued, and mania-like behavior in the elevated plus maze was only partially rescued.

From this we concluded that cortical behaviors were more amenable to functional recovery than subcortical behaviors. This was further studied with behaviors that engage the cortex and striatum, locomotor activity and stereotypy, and slice physiology of these two brain regions. We studied the electrophysiology of layer 5 cortical neurons in prefrontal cortex as well as medium spiny neurons in the dorsal striatum. Our interventions did not produce a recovery of NMDA receptor currents in the medium spiny neurons, which likely explains why stereotypy and locomotor activity were only modestly improved. However, the locomotor pattern of GluN1Cre mice showed a complete rescue of habituation. This may be due in part to the substantial recovery of NMDA current in cortical neurons.

An interesting parallel of our study can be made with the adult rescue of Shank3 deficiency. Shank3 is a scaffolding protein in excitatory synapses, and is in a larger complex with the post-synaptic density that includes NMDA receptors. When Shank3

deficiency is ameliorated at 8-18 weeks of age, social interactions are normalized, but hyperlocomotion and stereotypy are not (Mei et al., 2016). It would be interesting to discover whether higher-order cognition is also recovered, which would further the parallel between these models.

A number of studies have emphasized the vulnerability of the developing brain to NMDAR impairments, with early postnatal development a particularly critical time (Belforte et al., 2009; Crair and Malenka, 1995). Naturally, these findings have focused attention on the necessity for early intervention to better improve outcomes in schizophrenia treatment (Hadar et al., 2017; Laurens and Cullen, 2015). Indeed, we hypothesized that early intervention may be the key to improving cognition and social interactions, which are traditionally treatment-resistant. However, early intervention did not improve outcomes, and cognitive behaviors showed the highest levels of adult plasticity. If findings in mice are extended to humans, there is now reason to expect that cognitive and negative symptoms of schizophrenia could be dramatically ameliorated in adult patients with the right type of intervention and target.

Identifying such an intervention remains a challenge. Towards this goal, we investigated the molecular signature of NMDAR hypofunction and recovery using RNAseq. We found that many of the genes affected by NMDAR hypofunction participated in the biological processes of neurogenesis and neuronal fate commitment. Neurodevelopmental genes have been implicated in schizophrenia by genetic association studies (Walsh et al., 2008), but the assumption is that their pathogenic role occurs during early brain

development. The alteration of these pathways in the adult cortex of GluN1 knockdown mice suggests that NMDAR hypofunction may affect adult functions of neurogenesis-related genes, which may reshape the glial environment and provide trophic support for neuronal remodelling (Duan et al., 2015; Noristani et al., 2016). We speculate that the role of neurogenesis-genes in schizophrenia may be related to their adult brain functions, as has been suggested by the expression profiles of GWAS-susceptibility genes (Pers et al., 2016).

In conclusion, we have established that cortical circuits associated with negative symptoms are highly plastic in the adult brain. The failure of current antipsychotics to treat these symptoms is likely not a question of timing. When effective drugs are identified that target cortical circuits, there is promise that the underlying deficits can be overcome.

Author Contributions

Conceptualization, C.A.M., A.S., and A.J.R.; Methodology, C.A.M., Y.C., M.A.B., E.K.L., and A.J.R.; Formal Analysis, C.A.M., Y.C., M.A.B., E.K.L., and A.J.R.; Investigation, C.A.M., Y.C., M.A.B., R.I., M.M., and W.H.; Resources, A.S., E.K.L., and A.J.R.; Writing-Original Draft, C.A.M. and A.J.R.; Writing-Review & Editing, C.A.M., M.A.B., E.K.L., and A.J.R.; Visualization, C.A.M., M.A.B., and Y.C.; Supervision, E.K.L. and A.J.R.; Funding Acquisition, A.S., E.K.L., and A.J.R.

Acknowledgments

The authors would like to acknowledge Beverly Koller for donation of the pXena targeting construct, and Michael Didriksen, Jean-Martin Beaulieu, and Stephane Angers for helpful conversation. This work was supported by Operating Grants from CIHR to AJR (MOP119298), EKL (MOP89825) and AS (MOP206649).

REFERENCES

Afgan, E., Baker, D., van den Beek, M., Blankenberg, D., Bouvier, D., Čech, M., Chilton, J., Clements, D., Coraor, N., Eberhard, C., et al. (2016). The Galaxy platform for accessible, reproducible and collaborative biomedical analyses: 2016 update. Nucleic Acids Res. *44*, W3–W10.

Barres, B.A., Raff, M.C., Gaese, F., Bartke, I., Dechant, G., and Barde, Y.A. (1994). A crucial role for neurotrophin-3 in oligodendrocyte development. Nature *367*, 371–375.

Belforte, J.E., Zsiros, V., Sklar, E.R., Jiang, Z., Yu, G., Li, Y., Quinlan, E.M., and Nakazawa, K. (2009). Postnatal NMDA receptor ablation in corticolimbic interneurons confers schizophrenia-like phenotypes. Nature Neuroscience *13*, 76–83.

Ben Abdallah, N.M.B., Fuss, J., Trusel, M., Galsworthy, M.J., Bobsin, K., Colacicco, G., Deacon, R.M.J., Riva, M.A., Kellendonk, C., Sprengel, R., et al. (2011). The puzzle box as a simple and efficient behavioral test for exploring impairments of general cognition and executive functions in mouse models of schizophrenia. Exp. Neurol. *227*, 42–52.

Bolivar, V.J., Caldarone, B.J., Reilly, A.A., and Flaherty, L. (2000). Habituation of activity in an open field: A survey of inbred strains and F1 hybrids. Behav. Genet. *30*, 285–293.

Chen, W., Shieh, C., Swanger, S.A., Tankovic, A., Au, M., McGuire, M., Tagliati, M., Graham, J.M., Madan-Khetarpal, S., Traynelis, S.F., et al. (2017). GRIN1 mutation associated with intellectual disability alters NMDA receptor trafficking and function. J. Hum. Genet. 1–9.

Cline, H.T., Debski, E.A., and Constantine-Paton, M. (1987). N-methyl-D-aspartate receptor antagonist desegregates eye-specific stripes. Proc Natl Acad Sci USA *84*, 4342–4345.

Condorelli, D.F., Salin, T., Dell'Albani, P., Mudò, G., Corsaro, M., Timmusk, T., Metsis, M., and Belluardo, N. (1995). Neurotrophins and theirtrk receptors in cultured cells of the glial lineage and in white matter of the central nervous system. J. Mol. Neurosci. *6*, 237–248.

Crair, M.C., and Malenka, R.C. (1995). A critical period for long-term potentiation at thalamocortical synapses. Nature *375*, 325–328.

Crawley, J.N. (2004). Designing mouse behavioral tasks relevant to autistic-like behaviors. Ment. Retard. Dev. Disabil. Res. Rev. *10*, 248–258.

de Lau, W., Peng, W.C., Gros, P., and Clevers, H. (2014). The R-spondin/Lgr5/Rnf43 module: regulator of Wnt signal strength. Genes Dev. *28*, 305–316.

Dennis, M., Spiegler, B.J., Juranek, J.J., Bigler, E.D., Snead, O.C., and Fletcher, J.M. (2013). Age, plasticity, and homeostasis in childhood brain disorders. Neurosci

Biobehav Rev *37*, 2760–2773.

Domowicz, M.S., Sanders, T.A., Ragsdale, C.W., and Schwartz, N.B. (2008). Aggrecan is expressed by embryonic brain glia and regulates astrocyte development. Dev. Biol. *315*, 114–124.

Duan, C.-L., Liu, C.-W., Shen, S.-W., Yu, Z., Mo, J.-L., Chen, X.-H., and Sun, F.-Y. (2015). Striatal astrocytes transdifferentiate into functional mature neurons following ischemic brain injury. Glia *63*, 1660–1670.

Duncan, G.E., Moy, S.S., Lieberman, J.A., and Koller, B.H. (2006). Typical and atypical antipsychotic drug effects on locomotor hyperactivity and deficits in sensorimotor gating in a genetic model of NMDA receptor hypofunction. Pharmacol Biochem Behav *85*, 481–491.

Duncan, G., Moy, S., Perez, A., Eddy, D., Zinzow, W., Lieberman, J., Snouwaert, J., and Koller, B. (2004). Deficits in sensorimotor gating and tests of social behavior in a genetic model of reduced NMDA receptor function. Behavioural Brain Research *153*, 507–519.

Dzirasa, K., Ramsey, A.J., Takahashi, D.Y., Stapleton, J., Potes, J.M., Williams, J.K., Gainetdinov, R.R., Sameshima, K., Caron, M.G., and Nicolelis, M.A.L. (2009). Hyperdopaminergia and NMDA receptor hypofunction disrupt neural phase signaling. Journal of Neuroscience *29*, 8215–8224.

Ehninger, D., Li, W., Fox, K., Stryker, M., and Silva, A. (2008). Reversing neurodevelopmental disorders in adults. Neuron *60*, 950–960.

Ferris, M.J., Milenkovic, M., Liu, S., Mielnik, C.A., Beerepoot, P., John, C.E., España, R.A., Sotnikova, T.D., Gainetdinov, R.R., Borgland, S.L., et al. (2014). Sustained N-methyl-d-aspartate receptor hypofunction remodels the dopamine system and impairs phasic signaling. Eur J Neurosci 1–9.

Gainetdinov, R.R., Mohn, A.R., Bohn, L.M., and Caron, M.G. (2001). Glutamatergic modulation of hyperactivity in mice lacking the dopamine transporter. Proc Natl Acad Sci USA *98*, 11047–11054.

Gandal, M.J., Anderson, R.L., Billingslea, E.N., Carlson, G.C., Roberts, T.P.L., and Siegel, S.J. (2012). Mice with reduced NMDA receptor expression: more consistent with autism than schizophrenia? Genes Brain Behav *11*, 740–750.

Gazzerro, E., Smerdel-Ramoya, A., Zanotti, S., Stadmeyer, L., Durant, D., Economides, A.N., and Canalis, E. (2007). Conditional deletion of gremlin causes a transient increase in bone formation and bone mass. J. Biol. Chem. *282*, 31549–31557.

Giros, B., Jaber, M., Jones, S.R., Wightman, R.M., and Caron, M.G. (1996). Hyperlocomotion and indifference to cocaine and amphetamine in mice lacking the dopamine transporter. Nature *379*, 606–612.

Gogtay, N., Giedd, J.N., Lusk, L., Hayashi, K.M., Greenstein, D., Vaituzis, A.C., Nugent, T.F., Herman, D.H., Clasen, L.S., Toga, A.W., et al. (2004). Dynamic mapping of human cortical development during childhood through early adulthood. Proc Natl Acad Sci USA *101*, 8174–8179.

Goodman, C.S., and Shatz, C.J. (1993). Developmental mechanisms that generate precise patterns of neuronal connectivity. Cell *72 Suppl*, 77–98.

Grannan, M.D., Mielnik, C.A., Moran, S.P., Gould, R.W., Ball, J., Lu, Z., Bubser, M., Ramsey, A.J., Abe, M., Cho, H.P., et al. (2016). Prefrontal Cortex-Mediated Impairments in a Genetic Model of NMDA Receptor Hypofunction Are Reversed by the Novel M1 PAM VU6004256. ACS Chem Neurosci *7*, 1706–1716.

Hadar, R., Bikovski, L., Soto-Montenegro, M.L., Schimke, J., Maier, P., Ewing, S., Voget, M., Wieske, F., Götz, T., Desco, M., et al. (2017). Early neuromodulation prevents the development of brain and behavioral abnormalities in a rodent model of schizophrenia. Mol Psychiatry *00*, 1–9.

Halene, T.B., Ehrlichman, R.S., Liang, Y., Christian, E.P., Jonak, G.J., Gur, T.L., Blendy, J.A., Dow, H.C., Brodkin, E.S., Schneider, F., et al. (2009). Assessment of NMDA receptor NR1 subunit hypofunction in mice as a model for schizophrenia. Genes Brain Behav *8*, 661–675.

Han, S., Tai, C., Jones, C.J., Scheuer, T., and Catterall, W.A. (2014). Enhancement of Inhibitory Neurotransmission by GABAA Receptors Having α2,3-Subunits Ameliorates Behavioral Deficits in a Mouse Model of Autism. Neuron *81*, 1282–1289.

Hardingham, G.E., and Do, K.Q. (2016). Linking early-life NMDAR hypofunction and oxidative stress in schizophrenia pathogenesis. Nat Rev Neurosci *17*, 125–134.

Hubel, D.H., and Wiesel, T.N. (1963). Receptive fields of cells in striate cortex of very young, visually inexperienced kittens. J Neurophysiol 995–1002.

Huh, K.H., and Wenthold, R.J. (1999). Turnover analysis of glutamate receptors identifies a rapidly degraded pool of the N-methyl-D-aspartate receptor subunit, NR1, in cultured cerebellar granule cells. J. Biol. Chem. *274*, 151–157.

Islam, R., Trépanier, M.O., and Milenkovic, M. (2017). Vulnerability to omega-3 deprivation in a mouse model of NMDA receptor hypofunction. Npj Schizophrenia *3*.

Kamburov, A., Pentchev, K., Galicka, H., Wierling, C., Lehrach, H., and Herwig, R. (2011). ConsensusPathDB: toward a more complete picture of cell biology. Nucleic Acids Res. *39*, D712–D717.

Karolchik, D., Hinrichs, A.S., Furey, T.S., Roskin, K.M., Sugnet, C.W., Haussler, D., and Kent, W.J. (2004). The UCSC Table Browser data retrieval tool. Nucleic Acids Res. *32*, D493–D496.

Kent, W.J., Sugnet, C.W., Furey, T.S., Roskin, K.M., Pringle, T.H., Zahler, A.M., and Haussler, D. (2002). The human genome browser at UCSC. Genome Res. *12*, 996–1006.

Kirshenbaum, G.S., Clapcote, S.J., Duffy, S., Burgess, C.R., Petersen, J., Jarowek, K.J., Yücel, Y.H., Cortez, M.A., Snead, O.C., Vilsen, B., et al. (2011). Mania-like behavior induced by genetic dysfunction of the neuron-specific Na+,K+-ATPase α3 sodium pump. Proceedings of the National Academy of Sciences *108*, 18144–18149.

Kovacic, P., and Somanathan, R. (2010). Clinical physiology and mechanism of dizocilpine (MK-801): electron transfer, radicals, redox metabolites and bioactivity. Oxid Med Cell Longev *3*, 13–22.

Kwon, H.S., Nakaya, N., Abu-Asab, M., Kim, H.S., and Tomarev, S.I. (2014). Myocilin is involved in NgR1/Lingo-1-mediated oligodendrocyte differentiation and myelination of the optic nerve. Journal of Neuroscience *34*, 5539–5551.

Laurens, K.R., and Cullen, A.E. (2015). Toward earlier identification and preventative intervention in schizophrenia: evidence from the London Child Health and Development Study. Social Psychiatry and Psychiatric Epidemiology *51*, 475–491.

Lerner, T.N., and Kreitzer, A.C. (2011). Neuromodulatory control of striatal plasticity and behavior. Current Opinion in Neurobiology *21*, 322–327.

Leussis, M.P., and Bolivar, V.J. (2006). Habituation in rodents: a review of behavior, neurobiology, and genetics. Neurosci Biobehav Rev *30*, 1045–1064.

Li, N., Lee, B., Liu, R.-J., Banasr, M., Dwyer, J.M., Iwata, M., Li, X.-Y., Aghajanian, G., and Duman, R.S. (2010). mTOR-dependent synapse formation underlies the rapid antidepressant effects of NMDA antagonists. Science *329*, 959–964.

Li, P., Snyder, G.L., and Vanover, K.E. (2016). Dopamine Targeting Drugs for the Treatment of Schizophrenia: Past, Present and Future. Curr Top Med Chem *16*, 3385–3403.

Li, S., Cullen, W.K., Anwyl, R., and Rowan, M.J. (2003). Dopamine-dependent facilitation of LTP induction in hippocampal CA1 by exposure to spatial novelty. Nature Neuroscience *6*, 526–531.

Li, Y., Erzurumlu, R.S., Chen, C., Jhaveri, S., and Tonegawa, S. (1994). Whisker-related neuronal patterns fail to develop in the trigeminal brainstem nuclei of NMDAR1 knockout mice. Cell *76*, 427–437.

Lister, R.G. (1987). The use of a plus-maze to measure anxiety in the mouse. Psychopharmacology *92*, 180–185.

Lüdtke, T.H., Rudat, C., Wojahn, I., Weiss, A.-C., Kleppa, M.-J., Kurz, J., Farin, H.F., Moon, A., Christoffels, V.M., and Kispert, A. (2016). Tbx2 and Tbx3 Act Downstream of

Shh to Maintain Canonical Wnt Signaling during Branching Morphogenesis of the Murine Lung. Dev. Cell *39*, 239–253.

Ma, Y.-X., Wu, Z.-Q., Feng, Y.-J., Xiao, Z.-C., Qin, X.-L., and Ma, Q.-H. (2015). G protein coupled receptor 50 promotes self-renewal and neuronal differentiation of embryonic neural progenitor cells through regulation of notch and wnt/β-catenin signalings. Biochem. Biophys. Res. Commun. *458*, 836–842.

Madisen, L., Zwingman, T.A., Sunkin, S.M., Oh, S.W., Zariwala, H.A., Gu, H., Ng, L.L., Palmiter, R.D., Hawrylycz, M.J., Jones, A.R., et al. (2010). A robust and high-throughput Cre reporting and characterization system for the whole mouse brain. Nature Neuroscience *13*, 133–140.

Magnusson, K.R. (1995). Differential effects of aging on binding sites of the activated NMDA receptor complex in mice. Mech. Ageing Dev. *84*, 227–243.

McCoy, E., and Sontheimer, H. (2010). MAPK induces AQP1 expression in astrocytes following injury. Glia *58*, 209–217.

Mei, Y., Monteiro, P., Zhou, Y., Kim, J.-A., Gao, X., Fu, Z., and Feng, G. (2016). Adult restoration of Shank3 expression rescues selective autistic-like phenotypes. Nature *530*, 481–484.

Mielnik, C.A., Horsfall, W., and Ramsey, A.J. (2014). Diazepam improves aspects of social behaviour and neuron activation in NMDA receptor-deficient mice. Genes Brain Behav *13*, 592–602.

Mikell, C.B., Sheehy, J.P., Youngerman, B.E., McGovern, R.A., Wojtasiewicz, T.J., Chan, A.K., Pullman, S.L., Yu, Q., Goodman, R.R., Schevon, C.A., et al. (2014). Features and timing of the response of single neurons to novelty in the substantia nigra. Brain Research *1542*, 79–84.

Milenkovic, M., Mielnik, C.A., and Ramsey, A.J. (2014). NMDA receptor-deficient mice display sexual dimorphism in the onset and severity of behavioural abnormalities. Genes Brain Behav *13*, 850–862.

Miller, K.D., Chapman, B., and Stryker, M.P. (1989). Visual responses in adult cat visual cortex depend on N-methyl-D-aspartate receptors. Proc Natl Acad Sci USA *86*, 5183–5187.

Mohn, A., Gainetdinov, R., Caron, M., and Koller, B. (1999). Mice with reduced NMDA receptor expression display behaviors related to schizophrenia. Cell *98*, 427–436.

Monteiro, P., and Feng, G. (2016). Learning From Animal Models of Obsessive-Compulsive Disorder. Biological Psychiatry *79*, 7–16.

Moy, S.S., Nadler, J.J., Young, N.B., Perez, A., Holloway, L.P., Barbaro, R.P., Barbaro, J.R., Wilson, L.M., Threadgill, D.W., Lauder, J.M., et al. (2007). Mouse behavioral tasks

relevant to autism: phenotypes of 10 inbred strains. Behavioural Brain Research *176*, 4–20.

Moy, S.S., Nikolova, V.D., Riddick, N.V., Baker, L.K., and Koller, B.H. (2012). Preweaning Sensorimotor Deficits and Adolescent Hypersociability in Grin1 Knockdown Mice. Dev Neurosci *34*, 159–173.

Moy, S.S., Perez, A., Koller, B.H., and Duncan, G.E. (2006). Amphetamine-induced disruption of prepulse inhibition in mice with reduced NMDA receptor function. Brain Research *1089*, 186–194.

Nakashima, H., Ohkawara, B., Ishigaki, S., Fukudome, T., Ito, K., Tsushima, M., Konishi, H., Okuno, T., Yoshimura, T., Ito, M., et al. (2016). R-spondin 2 promotes acetylcholine receptor clustering at the neuromuscular junction via Lgr5. Sci Rep *6*, 28512.

Noristani, H.N., Sabourin, J.C., Boukhaddaoui, H., Chan-Seng, E., Gerber, Y.N., and Perrin, F.E. (2016). Spinal cord injury induces astroglial conversion towards neuronal lineage. Mol Neurodegener *11*, 68.

O'Connor, E.C., Bariselli, S., and Bellone, C. (2014). Synaptic basis of social dysfunction: a focus on postsynaptic proteins linking group-I mGluRs with AMPARs and NMDARs. Eur J Neurosci *39*, 1114–1129.

Paylor, R., and Crawley, J.N. (1997). Inbred strain differences in prepulse inhibition of the mouse startle response. Psychopharmacology *132*, 169–180.

Pers, T.H., Timshel, P., Ripke, S., Lent, S., Sullivan, P.F., O'Donovan, M.C., Franke, L., Hirschhorn, J.N., Schizophrenia Working Group of the Psychiatric Genomics Consortium (2016). Comprehensive analysis of schizophrenia-associated loci highlights ion channel pathways and biologically plausible candidate causal genes. Hum. Mol. Genet. *25*, 1247–1254.

Roybal, K., Theobold, D., Graham, A., DiNieri, J.A., Russo, S.J., Krishnan, V., Chakravarty, S., Peevey, J., Oehrlein, N., Birnbaum, S., et al. (2007). Mania-like behavior induced by disruption of CLOCK. Proc Natl Acad Sci USA *104*, 6406–6411.

Sale, A., Berardi, N., and Maffei, L. (2014). Environment and brain plasticity: towards an endogenous pharmacotherapy. Physiol Rev *94*, 189–234.

Schizophrenia Working Group of the Psychiatric Genomics Consortium (2014). Biological insights from 108 schizophrenia-associated genetic loci. Nature *511*, 421–427.

Shaw, P., Kabani, N.J., Lerch, J.P., Eckstrand, K., Lenroot, R., Gogtay, N., Greenstein, D., Clasen, L., Evans, A., Rapoport, J.L., et al. (2008). Neurodevelopmental trajectories of the human cerebral cortex. Journal of Neuroscience *28*, 3586–3594.

Sisk, C.L., and Zehr, J.L. (2005). Pubertal hormones organize the adolescent brain and behavior. Frontiers in Neuroendocrinology *26*, 163–174.

Snyder, M.A., and Gao, W.-J. (2013). NMDA hypofunction as a convergence point for progression and symptoms of schizophrenia. Front Cell Neurosci *7*, 31.

Stewart, S., Gomez, A.W., Armstrong, B.E., Henner, A., and Stankunas, K. (2014). Sequential and opposing activities of Wnt and BMP coordinate zebrafish bone regeneration. Cell Rep *6*, 482–498.

Swerdlow, N.R., Hanlon, F.M., Henning, L., Kim, Y.K., Gaudet, I., and Halim, N.D. (2001). Regulation of sensorimotor gating in rats by hippocampal NMDA: anatomical localization. Brain Research *898*, 195–203.

Szklarczyk, D., Franceschini, A., Wyder, S., Forslund, K., Heller, D., Huerta-Cepas, J., Simonovic, M., Roth, A., Santos, A., Tsafou, K.P., et al. (2015). STRING v10: protein-protein interaction networks, integrated over the tree of life. Nucleic Acids Res. *43*, D447–D452.

Tang, Y.P., Shimizu, E., Dube, G.R., Rampon, C., Kerchner, G.A., Zhuo, M., Liu, G., and Tsien, J.Z. (1999). Genetic enhancement of learning and memory in mice. Nature *401*, 63–69.

Tarabeux, J., Kebir, O., Gauthier, J., Hamdan, F.F., Xiong, L., Piton, A., Spiegelman, D., Henrion, É., Millet, B., S2D team, et al. (2011). Rare mutations in N-methyl-D-aspartate glutamate receptors in autism spectrum disorders and schizophrenia. Translational Psychiatry *1*, e55.

Trapnell, C., Roberts, A., Goff, L., Pertea, G., Kim, D., Kelley, D.R., Pimentel, H., Salzberg, S.L., Rinn, J.L., and Pachter, L. (2012). Differential gene and transcript expression analysis of RNA-seq experiments with TopHat and Cufflinks. Nat Protoc *7*, 562–578.

Traynelis, S.F., Wollmuth, L.P., McBain, C.J., Menniti, F.S., Vance, K.M., Ogden, K.K., Hansen, K.B., Yuan, H., Myers, S.J., and Dingledine, R. (2010). Glutamate receptor ion channels: structure, regulation, and function. Pharmacological Reviews *62*, 405–496.

Tsumoto, T., Hagihara, K., Sato, H., and Hata, Y. (1987). NMDA receptors in the visual cortex of young kittens are more effective than those of adult cats. Nature *327*, 513–514.

Uzunova, G., Hollander, E., and Shepherd, J. (2014). The role of ionotropic glutamate receptors in childhood neurodevelopmental disorders: autism spectrum disorders and fragile x syndrome. Curr Neuropharmacol *12*, 71–98.

van Os, J., and Kapur, S. (2009). Schizophrenia. Lancet *374*, 635–645.

Ventura, A., Kirsch, D.G., McLaughlin, M.E., Tuveson, D.A., Grimm, J., Lintault, L., Newman, J., Reczek, E.E., Weissleder, R., and Jacks, T. (2007). Restoration of p53 function leads to tumour regression in vivo. Nature *445*, 661–665.

Vogt, M.A., Chourbaji, S., Brandwein, C., Dormann, C., Sprengel, R., and Gass, P.

(2008). Suitability of tamoxifen-induced mutagenesis for behavioral phenotyping. Exp. Neurol. *211*, 25–33.

Walsh, T., McClellan, J.M., McCarthy, S.E., Addington, A.M., Pierce, S.B., Cooper, G.M., Nord, A.S., Kusenda, M., Malhotra, D., Bhandari, A., et al. (2008). Rare structural variants disrupt multiple genes in neurodevelopmental pathways in schizophrenia. Science *320*, 539–543.

Wang, W.-D., Melville, D.B., Montero-Balaguer, M., Hatzopoulos, A.K., and Knapik, E.W. (2011). Tfap2a and Foxd3 regulate early steps in the development of the neural crest progenitor population. Dev. Biol. *360*, 173–185.

Welch, J.M., Lu, J., Rodriguiz, R.M., Trotta, N.C., Peca, J., Ding, J.-D., Feliciano, C., Chen, M., Adams, J.P., Luo, J., et al. (2007). Cortico-striatal synaptic defects and OCD-like behaviours in Sapap3-mutant mice. Nature *448*, 894–900.

Wesseling, H., Guest, P.C., Lee, C.-M., Wong, E.H., Rahmoune, H., and Bahn, S. (2014). Integrative proteomic analysis of the NMDA NR1 knockdown mouse model reveals effects on central and peripheral pathways associated with schizophrenia and autism spectrum disorders. Mol Autism *5*, 38.

Yuan, H., Low, C.-M., Moody, O.A., Jenkins, A., and Traynelis, S.F. (2015). Ionotropic GABA and Glutamate Receptor Mutations and Human Neurologic Diseases. Molecular Pharmacology *88*, 203–217.

Zhang, L., Yin, J.-C., Yeh, H., Ma, N.-X., Lee, G., Chen, X.A., Wang, Y., Lin, L., Chen, L., Jin, P., et al. (2015). Small Molecules Efficiently Reprogram Human Astroglial Cells into Functional Neurons. Cell Stem Cell *17*, 735–747.

Zorumski, C.F., and Izumi, Y. (2012). NMDA receptors and metaplasticity: mechanisms and possible roles in neuropsychiatric disorders. Neurosci Biobehav Rev *36*, 989–1000.

FIGURE AND TABLE LEGENDS

Figure 1. Generation and validation of GluN1-inducible rescue mouse line (*Grin1*$^{flneo/flneo}$).

(A) Targeting construct schematic and recombination events at the *Grin1* locus in the generation of the *Grin1*$^{flneo/flneo}$ mouse model (top panel). PGK, PGK promotor; neo, neomycin selection cassette; polyA, polyadenylation sequence. (Lower panel) Schematic of expected molecular events at the *Grin1* locus.

(B) Image of cortex, striatum, hippocampus and cerebellum visualizing tdTomato expression following Cre-mediated recombination in *ROSA26*$^{CreERT2/tdTomato}$ mice treated with TAM or vehicle.

(C) Western blot of GluN1 and GluN2A protein from cortical tissue of mice treated with tamoxifen, quantified using total protein stain as loading control. Data shown as mean ± SEM, *p<0.05, **p<0.01, ***p<0.001, ****p<0.0001, one-way ANOVA, Bonferroni posthoc.

(D) Regimen of tamoxifen administration and subsequent analysis in three experimental groups. Red arrow, tamoxifen-induced Cre expression; black arrow, phenotype observation.

(E) Order of behavioral tests over five days.

Table 1. NMDA receptor binding densities of [^{3}H]MK-801 (fmol/mg) in brain tissue of WT, GluN1 and GluN1Cre mice.

Figure 2. Reversal of cognitive impairments, but only partial improvement of mania-like behavior.

(A) Schematic of puzzle box test. Time to reach goal zone (sec; max 300sec) measured in puzzle box paradigm in WT, GluN1, GluN1Cre mice. Shown on graph, WT vs. GluN1Cre: *p<0.05, **p<0.01, ***p<0.001, ****p<0.0001. Data shown as mean ± SEM, two-way ANOVA, effect of genotype, (Adolescent +8WR) $F_{3,84}$=57.829, (Adult +4WR) $F_{3,82}$=53.634, (Adult +8WR) $F_{3,81}$=56.479, Bonferroni posthoc.

(B) Representative traces of modified three-chamber sociability. Total time spent in zone over 10min. Data shown as mean ± SEM, *p<0.05, **p<0.01, ***p<0.001, ****p<0.0001, ns = not significant, one-way ANOVA (social zone), effect of genotype, (Adolescent +8WR) $F_{3,78}$=6.994, (Adult +4WR) $F_{3,75}$=7.140, (Adult +8WR) $F_{3,80}$=8.824, Bonferroni posthoc.

(C) Representative traces of elevated plus maze test. Percent time spent in open arms over 8min. Data shown as mean ± SEM, ****p<0.0001, one-way ANOVA, effect of genotype, (Adolescent +8WR) $F_{3,78}$=207.461, (Adult +4WR) $F_{3,75}$=252.955, (Adult +8WR) $F_{3,80}$=186.135, Bonferroni posthoc.

Figure 3. Differential recovery of cortical and subcortical behaviors.

(A) Percent inhibition of startle response (PPI; top panel) and acoustic startle response (ASR; lower panel). Shown on graph, GluN1 vs. GluN1Cre: **p<0.01, ***p<0.001, ****<0.0001, ns = not significant, data shown as mean ± SEM, one-way ANOVA, effect of genotype in PPI, (Adolescent +8WR) $F_{3,78}$=(4dB)11.236,

(8dB)1.119, (16dB)3.160, (Adult +4WR) $F_{3,75}$= (4dB)8.805, (8dB)14.594, (16db)9.571, (Adult +8WR) $F_{3,80}$=(4dB)20.029, (8dB)11.327, (16dB)6.034, Bonferroni posthoc.

(B) Time-course of distance traveled (left panel) and habituation (middle panel). Data shown as mean ± SEM, ****p<0.0001, two-way ANOVA (time-course), one-way ANOVA (habituation), effect of genotype, (Adolescent +8WR) $F_{3,160}$=227.955, (Adult +4WR) $F_{3,164}$=176.340, (Adult +8WR) $F_{3,168}$=339.428, Bonferroni posthoc.

(C) Total stereotypic movements. Data shown as mean ± SEM, ****p<0.0001, one-way ANOVA, effect of genotype, (Adolescent +8WR) $F_{3,160}$=459.259, (Adult +4WR) $F_{3,164}$=301.851, (Adult +8WR) $F_{3,168}$=537.974, Bonferroni posthoc.

Figure 4. NMDAR currents are restored in medial prefrontal cortex but not in the dorsal striatum.

(A) Schematic of medial prefrontal cortex with whole cell patch clamp recording from layer 5 (adapted from Paxinos & Franklin, 2001). Inset: electrophysiological signature of GluN1Cre layer 5 pyramidal neuron.

(B) Representative traces in voltage-clamp (-75 mV) showing prefrontal response to NMDA across the three genotypes (number of layer 5 pyramidal neurons shown, 5-6 mice per genotype).

(C) Quantification of peak amplitude of prefrontal NMDAR-elicited currents. Data shown as mean ± SEM, ****p<0.0001, ns =not significant, one-way ANOVA, effect of genotype, $F_{2,95}$ =22, p<0.0001, Bonferroni posthoc.

(D) Capacitance of prefrontal layer 5 pyramidal neurons. Data shown as mean ± SEM, *p<0.05, ns =not significant, one-way ANOVA, Bonferroni posthoc.

(E) Current density of prefrontal NMDA-elicited currents. Data shown as mean ± SEM, **p<0.01, ****p<0.0001, one-way ANOVA, effect of genotype, $F_{2,95}$ =3.6, p=0.03, Bonferroni posthoc.

(F) Schematic of dorsal striatum with whole cell patch clamp recording (adapted from Paxinos & Franklin, 2001). Inset: electrophysiological signature of a medium spiny neuron in GluN1Cre.

(G) Representative traces in voltage-clamp (-75 mV) showing striatal response to NMDA across the three genotypes (number of medium spiny neurons shown, 4-5 mice per genotype).

(H) Quantification of peak amplitude of NMDAR currents in medium spiny neurons. Data shown as mean ± SEM, **p<0.01, ****p<0.0001, ns =not significant, one-way ANOVA, effect of genotype, $F_{2,72}$ =13, p<0.0001, Bonferroni posthoc.

Table 2. Significantly altered biological processes due to GluN1 knockdown and rescue.

Figure 5. RNAseq identifies the molecular signatures of NMDAR deficiency and recovery

(A) Proportion of genes that are altered in GluN1 and are normalized in GluN1Cre mice. An additional 68 genes showed significantly altered expression only in GluN1Cre mice (unique).

(B) String network of genes in the biological process “neurogenesis” that are altered in GluN1 mice and are “rescue-responsive” (blue) or “rescue-resistant” (red) in GluN1Cre mice.

(C) List of 56 genes with a greater than two-fold change in expression in GluN1 mice compared to WT. Increased gene expression in GluN1 relative to WT is indicated by red color intensity, and decreased gene expression is indicated by blue color intensity. In GluN1Cre mice, all but one of the 56 genes normalized expression towards WT levels, as depicted by reduced color intensity.

STAR METHODS

- CONTACT FOR REAGENT AND RESOURCE SHARING
- EXPERIMENTAL MODEL AND SUBJECT DETAILS
    - Experimental Mouse Lines and Genotyping
- METHOD DETAILS
    - Tamoxifen Administration
    - Behavior Testing
    - Open Field Test
    - Puzzle Box Assay
    - Elevated Plus Maze
    - Social Affiliative Paradigm
    - Pre-Pulse Inhibition/Startle Reflex
    - Harvesting Whole Brain Tissue
    - Immunohistochemistry Cre Reporter
    - Immunoblotting
    - [3H]MK-801 Saturation Binding Assay
    - Electrophysiological recordings
    - RNA Isolation, Sequencing and Analysis
- QUANTIFICATION AND STATISTICAL ANALYSIS
- DATA AND SOFTWARE AVAILABILITY
- ADDITIONAL RESOURCES

Experimental Mouse Lines and Genotyping

Animal housing and experimentation were carried out in accordance with the Canadian Council in Animal Care (CCAC) guidelines for the care and use of animals. Mice were group housed with littermates on a 12-h light-dark cycle (0700 to 1900h) and were given access to food (2018 Teklad Global 18% Protein Rodent Diet, Envigo, Madison Wisconsin USA, www.envigo.com) *ad libitum*, unless otherwise specified. Mice were tail clipped and had their toes tattooed at P13 (± 3 days) for genotyping and weaned at P21. Toe tattooing was used to identify all experiment mice.

ROSA26^{CreERT2} (tamoxifen inducible) mice were obtained from Jackson Laboratory (008463; B6.129-*Gt(ROSA)26Sor*$^{tm1(cre/ERT2)Tyj}$*/J*), and were previously described (Ventura et al., 2007). The Cre gene was identified using the following primers: common forward 5'- AAA GTC GCT CTG AGT TGT TAT-3', wildtype reverse 5'- GGA GCG GGA GAA ATG GAT ATG-3', mutant reverse 5'- CCT GAT CCT GGC AAT TTC G-3'.

The Cre-reporter mouse line used, *ROSA26*^{tdTomato}, was obtained from Jackson Laboratory (007914; B6.Cg-*Gt(ROSA)26Sor*$^{tm14(CAG-tdTomato)Hze}$/J) and was crossed with the *ROSA26*^{CreERT2} line. The mouse line expressed tdTomato following Cre-mediated recombination. Mouse line was used to ensure ubiquitous expression of Cre following tamoxifen administration as was previously described (Madisen et al., 2010). The reporter gene was indentified using the following primers: wildtype forward 5'- AAG GGA GCT GCA GTG GAG TA-3', wildtype reverse 5'- CCG AAA ATC TGT GGG AAG

TC-3', mutant forward 5'- GGC ATT AAA GCA GCG TAT CC-3', mutant reverse 5'- CTG TTC CTG TAC GGC ATG G-3'.

Grin1$^{flneo/flneo}$ mice were generated in house, based on the previously described GluN1-knockdown mouse (Mohn et al., 1999). Identical to the GluN1-knockdown model, the *Grin1* gene was modified via homologous recombination with an intervening sequence (neomycin cassette), and targeted into intron 19, but this time flanked by *loxP* sites, so the insertion mutation could be excised following Cre-recombination (see Figure 1A). Concisely, the vector (pXena; construct was gift from Beverly Koller, UNC Chapel Hill, USA) contained a floxed neomycin resistance gene (insertion mutation, contains STOP codon as well as polyA sequence). Homologous arms (upstream – 5' and downstream – 3') of intron 19 of the *Grin1* gene were PCR-amplified from mouse genomic DNA and cloned into the vector flanking the floxed neomycin cassette. The construct was sequenced. Electroporation into mouse ES cells (129/SvlmJ strain) was completed by The Centre for Phenogenomics (TCP, Toronto, ON). ES cells were selected for with G418. Drug resistant clones were screened by PCR, and then further confirmed via Southern blot analysis (data not shown). Correctly targeted ES cell clones were injected into albino blastocysts (via diploid aggregation; TCP) to generate chimeras, and then bred with 129/SvlmJ female mice to obtain ES cell germline transmitted offspring, determined by black eye colour and PCR screening.

All experimental animals were of F1 progeny of *Grin1*$^{flneo/flneo}$ heterozygotes; C57Bl/6 background and 129/SvlmJ background. As the ES cells were on a 129/SvlmJ

background, germline transmitted offspring were crossed directly with 129/SvlmJ mice to create the *Grin1*$^{flneo/flneo}$ (129/SvlmJ) line. For the C57Bl/6 *Grin1*$^{flneo/flneo}$ line, mice were backcrossed for at least 6 generations. The floxed insertion mutation (neo) was identified using the following primers: wildtype forward 5'- TGA GGG GAA GCT CTT CCT GT-3', mutant forward 5'- GCT TCC TCG TGC TTT ACG GTA T-3', common reverse 5'-AAG CGA TTA GAC AAC TAA GGG T-3'.

Grin1$^{flneo/Cre}$ mice (*Grin1*$^{flneo/flneo}$ x *ROSA26*^{CreERT2}) were generated by having the *ROSA26*^{CreERT2} mice (C57Bl/6) bred to heterozygous *Grin1*$^{flneo/flneo}$ mice on the C57Bl/6 background. The compound heterozygotes (C57Bl/6) were bred back to the heterozygous *Grin1*$^{flneo/flneo}$ mice (129/SvlmJ) resulting in F1 progeny at the expected Mendelian frequency for all proposed studies; 12.5% WT, 12.5%WTCre, 12.5% GluN1 and 12.5% GluN1Cre. Primers mentioned above were used to identify the Cre gene and the *Grin1* insertion mutation.

Tamoxifen Administration

Tamoxifen was administered to all mice tested, in all genotypes (WT, WTCre, GluN1, GluN1Cre) of *Grin1*$^{flneo/Cre}$ mice. Tamoxifen (T5648, Sigma-Aldrich, St. Louis, MO, USA) was administered via oral gavage (6mg, 20mg/ml dissolved in 100% corn oil at 65°C) on day 1 of treatment, and then mice were given access to tamoxifen chow (TD.140425, 500mg/kg, Envigo) *ad libitum* for 14 days. Treatment with tamoxifen started at either 6- or 10-weeks, depending on treatment group (see Figure 1D). Following tamoxifen administration, nails were trimmed every 2-weeks on all mice tested to help prevent

confounding factors of potential scratching behavior. Mice did not display any health or behavior changes while on the tamoxifen diet.

Behavioral Testing

F1 male and female (balanced *n* for sex in each behavior) *Grin1*$^{flneo/Cre}$ mice were used for all behavioral testing. Testing was done at either 14-weeks (tamoxifen at 6- or 10-weeks) or 18-weeks (tamoxifen at 10-weeks), see Figure 1D. WT mice not expressing the Cre gene, but treated with tamoxifen, were used as littermate controls. All behavioral tests were completed between 09:00 and 15:00h. All mice were tested for locomotor activity and stereotypic behavior on the first day of behavioral assessment. Mice were then assigned to one of two groups for subsequent behavioral tests that spanned three days. (Figure 1E). Mice were assigned to one of two groups to ensure that all mice 1) were tested for the same total number of days, 2) sacrificed on the same day and, 3) were not tested for too long a period so as to minimize confounding stress effects. Days 2 through 4 saw group A tested in the puzzle box assay, while group B was tested in the elevated plus maze, social affiliative paradigm, and then pre-pulse inhibition.

Open Field Test

For all intervention time points, as well as both group A and B (see Figure 1E), locomotor activity and stereotypy were measured as previously described by (Milenkovic et al., 2014) using digital activity monitors (Omnitech Electronics, Columbus, OH, USA) on the first day of testing. Naïve mice were placed in novel Plexiglas arenas

(20 x 20 x 45 cm) and their locomotor and stereotypic activity were recorded over a 120-min period in dim light (15-16lux). Activity was tracked via infrared light beam sensors; total distance traveled and stereotypic movements were collected in 5-min bins.

Puzzle Box Assay

For all intervention time points in group A (see Figure 1E), mice were run on the Puzzle Box Assay on days 2-4 of testing to assess cognition and executive function, (adapted from (Ben Abdallah et al., 2011), as previously described by (Milenkovic et al., 2014). Consisting of two compartments, the puzzle box contains a start area (58 x 28 x 27.5 cm) in bright light (250lux), and a goal zone (14 x 28 x 27.5 cm) in dim light (5lux). The two areas separated by a black Plexiglas divider, but connected via an underpass large enough for mice to pass through easily. Mice were placed in the start box facing away from the divider and the time to move to the goal zone (through the underpass, with both hind legs in the goal zone) was manually scored and recorded. Mice were tested over three days, 3 trials/day (except 1 trial on day 3), with each day consisting of increasingly difficult obstacles present in the underpass connecting the start area and the goal zone. 2-min. were given between each trial on a given day, with a max 300-sec. allowed for the completion of each trial.

The trials (and obstacles) for the puzzle box were as follows;

Day 1: T1 (training) open door and unblocked underpass, T2 and T3 (challenge, then learning) door way closed and underpass open

Day 2: T4 (explicit memory) identical trial to T3, T5 and T6 (challenge, then learning) underpass filled with bedding (similar to that found in home cage)

Day 3: T7 (explicit memory) identical trial to T6

Elevated Plus Maze

For group B (see Figure 1E), anxiety behavior was assessed on day 2 of testing via elevated plus maze (Moy et al., 2007). The elevated plus maze was composed of 4 opaque-white arms (2 opposite arms closed, 2 opposite arms open), arranged in a plus shape, with an open center. The dimensions were as follows; maze elevation (38.7cm), open arm (L:30.5cm, W:5cm, H:0cm), closed arm (L:30.5cm, W:5cm, H:15.2cm) and center (5cm x 5cm). The experiment mouse was placed in the center of the maze, and allowed to freely explore the maze for 8-min in dim light (15-16lux), while being tracked with an overhead camera. Open and closed arm times were recorded and collected by Biobserve Viewer3 software. The percentage of time spent in the open arms as compared to closed arms and center time was calculated and expressed as a percent of time spent in the open arms of the maze.

Social Affiliative Paradigm

For group B (see Figure 1E), social affiliative behavior was assessed on day 3 of testing, as previously described by (Mielnik et al., 2014) and (Milenkovic et al., 2014). Sociability was measured via video recording motion and exploration of experimental mouse tracked via Biobserve Viewer (version 2) software (center body – reference point). Experimental mice were allowed to explore the open area (opaque white walls, 62 x 42

x 22 cm) for 10-min in dim lighting (15-16lux). The area contained two inverted wire cups, one containing a stimulus mouse (‘social’) and the other empty (‘non-social’). Time spent in each zone (3cm zone around the cup) was recorded via the Biobserve software. Mice used as a social stimulus were novel, wildtype, inbred C57Bl/6 mice that were age- and sex-matched to the test mouse.

Pre-Pulse Inhibition/Startle Reflex

For group B (see Figure 1E), pre-pulse inhibition of the acoustic startle response was measured on day 4, via SR-LAB equipment and software from San Diego Instruments. Accelerometers were calibrated to 700±5 mV and output voltages were amplified and analyzed for voltage changes using SR Analysis (San Diego Instruments, San Diego, CA, USA), and exported as an excel file. Background white noise was maintained at 65dB. PPI was measured in a 30-min test with 80 randomized trials of: (1) 10 trials pulse alone (2) 10 trials pre-pulse alone (for each pre-pulse), (3) 10 trials pre-pulse plus pulse (for each pre-pulse), and (4) 10 trials no pulse. 5 pulse alone trials were performed before and after the 80 trials, totaling 90 trials per run. The pre-pulse (4dB, 8dB, or 16dB) was presented 100ms prior to the startle pulse (165dB). The inter-stimulus interval (ISI) was randomized between 5 and 20s. Experimental mice were placed in a cylindrical tube on a platform in a soundproof chamber. Mice were allowed to acclimatize in the chamber and to the background noise for 300s, followed by 5 consecutive pulse alone trials, then by 80 randomized trials (as described above) and then 5 consecutive pulse alone trials. Pre-pulse inhibition was measured as a decrease

in the amplitude of startle response to a 100dB acoustic startle pulse, following each pre-pulse (4dB, 8dB and 16dB).

Harvesting Whole Brain Tissue

On Day 5, following all behavioral testing, mice were sacrificed via live cervical dislocation. Brains were removed and frozen in ice cold isopentane (sitting on dry ice). Brains were then put into 5ml eppendorf tubes and stored at -80°C until further use.

Immunohistochemistry Cre Reporter (*ROSA26*^{tdTomato} x *ROSA26*^{CreERT2})

Mice were treated with tamoxifen for 2-weeks (as previously described) and anaesthetized (250mg/kg Avertin, [2,2,2-tribromoethanol (Sigma Aldrich) dissolved in 2-methyl-2-butanol (Sigma Aldrich), 2.5% v/v)] 3 days following last day of treatment. Whole brains were perfused with 4% paraformaldehyde (PFA), post-fixed in PFA for 3 hours at 4°C and then transferred to 30% sucrose for 3 days at 4°C. Fixed brains were sectioned at 40µm coronal sections (around Bregma 1.78mm, 1.10mm, -1.94mm, -6.00mm). Sections were mounted and visualized using Nikon Elements software (NIS-Elements Basic Research, version 3.1).

Immunoblotting

Prefrontal cortex tissue was dissected from brains frozen in cold isopentane (over dry ice, previously described). Tissue homogenates were prepared according to (Li et al., 2010). Tissue was homogenized in homogenization solution (0.32M sucrose, 20mM HEPES pH 7.4, 1mM EDTA) for 30-sec with a hand-held motorized pestle. At 4°C,

homogenate was spun at 1000G for 10-min, and then supernatant spun at 10000G 10-min. Pellet was resuspended in lysis buffer (50mM Tris HCl pH7.5, 150mM NaCl, 1% Triton X-100, 0.1% SDS, 2mM EDTA). Protein concentration was measured using BCA assay (Thermo Scientific). Proteins were resolved on 4% stacking and 8% separating gels and transferred to PVDF membranes (Pall Life Sciences, NY, USA) via 1 hour transfer at 100V. Total protein was stained for using REVERT™ Total Protein Stain Kit (LI-COR, Lincoln, NE, USA). Membranes were blocked in 5% milk in TBS-T (TBS + 0.1% (v/v) Tween-20) for 30-min and then incubated in primary antibodies (in 5% milk in TBS-T) overnight at 4°C. Primary antibodies for NR1 and NR2A proteins are as follows:

NR1 – 1:250, mouse IgG, Upstate (Millipore) Cat No: 05-432, Lot: 2538

NR2A – 1:1000, rabbit IgG, Upstate (Millipore) Cat No: 07-632, Lot: 32704

Blots were washed in TBS-T, incubated with anti-mouse IRDye 680 (1:10000, LI-COR) and anti-rabbit IRDye 800 (1:10000, LI-COR). Blots were visualized and densitometry was analyzed using the LI-COR Odyssey system and software.

[^{3}H]MK-801 Saturation Binding Assay

Prefrontal cortical, striatal, hippocampal and cerebellar tissue was dissected from whole frozen brains (see previous section). To ensure sufficient protein for total protein radioligand binding (total 400ug of protein needed), each brain region was pooled from two separate animals (ex: 2 cortical regions from two separate mice were pooled for a single n, within each genotype).

To prepare membranes, tissue was homogenized in binding buffer (20mM HEPES pH 7.4, 1mM EDTA pH 8.0, 0.1mM glycine, 0.1mM glutamate, 0.1mM spermidine, Aprotinin (1000x), Leupeptin (1000x), Pepstatin A (500x), Benzamidine (1000x) and PMSF (2500x)) using a standing homogenizer and glass Teflon homogenizer tubes. Homogenate was transferred to 12ml round bottom tubes and further homogenized (Polytron, PT-1200-E). Homogenate was cleared via centrifugation at 600G in Sorvall SM-24 rotor for 10-min at 4°C. Supernatant was transferred to thick walled Sorvall tubes and cleared via centrifugation at 40000G in Sorvall SM-24 rotor for 15-min at 4°C. Pellet was washed with binding buffer (without protease inhibitors) and re-cleared at 40000G in Sorvall SM-24 rotor for 15-min at 4°C. Pellets were resuspended in binding buffer (without protease inhibitors). Protein concentration was measured using BCA assay (Thermo Scientific). Membranes were diluted to a 1.6µg/µl working concentration and stored at -80°C.

For the [^{3}H]MK-801 saturation protein binding assay, working solutions of [^{3}H]MK-801 and cold MK-801 were prepared. [^{3}H]MK-801 (Perkin Elmer) was diluted to a working concentration of 120nM (final concentration 40nM) in binding buffer. Cold MK-801 (Sigma Aldrich) was prepared to a 1200nM working solution (final concentration 400nM; 10x [^{3}H]MK-801) in binding buffer. Binding assays were performed with the NMDAR antagonist MK-801 (hot and/or cold), mouse brain membranes (80µg) and binding buffer (total binding vs. non-specific binding), with a total assay volume of 150µl. Assays were carried out at 32°C for 3 hours in a shaking water bath before termination by the addition of ice-cold wash buffer (20mM HEPES pH 7.4, 1mM EDTA pH 8.0) and

vacuum filtration using a 24-well sampling manifold (Brandel Cell Harvester) and Whatman GF/B glass-fibre filters (Brandel, MD, USA) that had been soaked in 0.05% polyethylenimine for 30-min. Each reaction was washed 5 times with wash buffer. Filters were placed in 5mL scintillation fluid (Ultima Gold XR, Perkin Elmer) and allowed to incubate overnight. Radioactivity was quantified via liquid scintillation spectrometry.

Electrophysiological recordings

Mice from the three genotypes (Adult +4WR) were administered chloral hydrate (400 mg/kg) and sacrificed. The brain was removed from the skull and cooled in oxygenated sucrose-substituted ACSF. The brain was blocked to obtain the anterior portion and coronal slices (400 µm) of the medial prefrontal cortex (1.98 mm-1.34 mm; Paxinos & Franklin Atlas) and caudate putamen (1.54 mm - 0.14 mm; Paxinos & Franklin Atlas) were sectioned by the Dosaka Pro-7 Linear Slicer (SciMedia). The slices recovered for at least 1.5 hours in a chamber containing oxygenated ACSF (in mM: 128 NaCl, 10 D-glucose, 26 $NaHCO_3$, 2 $CaCl_2$, 1.25 NaH_2PO_4, 2 $MgSO_4$, 3 KCl) at 30°C before being transferred to the stage of an upright microscope for whole cell patch clamp recordings. Layer V pyramidal neurons in the medial prefrontal cortex and medium spiny neurons in the dorsal striatum were identified by infrared differential inference contrast microscopy. The whole cell patch pipettes (2-4 MΩ) contained the following intracellular solution (in mM): 120 potassium gluconate, 5 KCl, 2 MgCl, 4 K_2-ATP, 0.4 Na_2-GTP, 10 Na_2-phosphocreatine, and 10 HEPES buffer, adjusted to pH 7.33 with KOH.

For these experiments, the brain slices were continuously perfused with 30°C modified ACSF (in mM: 128 NaCl, 10 D-glucose, 26 $NaHCO_3$, 2 $CaCl_2$, 1.25 NaH_2PO_4, 0.5 $MgSO_4$, 5 KCl) to relieve the magnesium blockade in order to study NMDARs. Experiments were performed in the presence of CNQX disodium salt (20 µm; Alomone Labs) to block AMPA receptors. NMDA (30 µm; Sigma-Aldrich) was bath applied to assess NMDAR function. Application of APV (50 µM; Alomone Labs) confirmed the inward currents were mediated by NMDARs. The peak amplitude of the NMDA currents was measured using Clampfit software (Molecular Devices). The magnitude of NMDA-elicited inward currents was quantified by subtracting a 1 second average holding current at the peak from the average holding current at the baseline.

RNA Isolation, Sequencing and Analysis

Total RNA for RNAseq was isolated from frozen, homogenized cortical tissue from male mice treated at 10-weeks with tamoxifen (see section ‘Tamoxifen Administration’) and sacrificed at 14-weeks. Four mice were included for each genotype. RNA was isolated with Tri Reagent (BioShop Canada) followed by purity verification via OD260/OD280 ratios taken by an Epoch Microplate Spectrophotometer (BioTek, VT, USA). 2-6µg of RNA was aliquoted for each sample and sent to The Centre for Applied Genomics (TCAG; Toronto, Canada) for RNA sequencing and the generation of raw sequence reads using the Illumina HiSeq 2500 protocol (Illumina, CA, USA). Poly-A isolation, library generation, amplification and sequencing were performed by TCAG.

RNAseq data was analyzed with the tuxedo protocol originally described by (Trapnell et al., 2012) using the main public online Galaxy platform (Afgan et al., 2016). Briefly, RNAseq reads for each sample were first quality checked with FastQC (version 0.65), followed by preparation for use on Galaxy with FASTQ Groomer (Version 1.0.4) and GRCm38/mm10 mouse genome alignment with TopHat (Version 2.1.0). The aligned reads were then assembled into transcripts with Cufflinks (Version 2.2.1.0) using a mouse RefSeq annotation from the National Center for Biotechnology Information (NCBI) as an annotation guide. The transcripts assembled for each sample were then combined with Cuffmerge (Version 2.2.1.0). The resulting genome annotation was used to quantify and compare WT vs GluN1 vs GluN1Cre gene expression in Cuffdiff (Version 2.2.1.3) via three pairwise comparisons due to limitations of computing resources. Significance thresholds were set at p and q (false discovery rate) values of 0.05 and 0.1, respectively.

Significant gene differential comparison results from all three pairwise RNAseq runs were combined and aligned to match gene name, loci, and transcription start sites as much as possible. Unrecognized entries were checked again for an identifier using their loci with the Refseq database in the University of California, Santa Cruz genome table browser (Karolchik et al., 2004; Kent et al., 2002). Identified genetic elements were analyzed with ConsensusPathDB's gene set over-representation analysis to determine enriched biological processes in level 5 gene ontology categories (Kamburov et al., 2011). The genes belonging to the neurogenesis biological process were visualized using STRINGDB (Szklarczyk et al., 2015).

Quantification and Statistical Analysis

Statistical parameters, including the exact value of n, the definition of measures and statistical significance are reported in the Figures and the Figure Legends. Data are represented as mean ± SEM, as indicated in figure legends. Sample number (*n*), indicating independent biological samples (balanced for sex), are indicated in each figure and/or figure legend. Data were analyzed either using a one- or two-way ANOVA (repeated measures) where indicated, with multiple comparisons and post-hoc Bonferroni's test, as indicated in figure legends. For electrophysiological recordings, paired t-tests were used to compare neuronal responses to NMDA before and after APV. Data analysis was not blinded. Differences in means were considered statistically significant at $p<0.05$. Significance levels are as follows; *$p<0.05$, **$p<0.01$, ***$p<0.001$, ****$p<0.0001$, ns – not significant. All data analyses were performed using the Graphpad Prism 6.0 software and/or IBM SPSS 23.0 Software.

Data Software Availability

Raw data files for the RNA sequencing analysis have been deposited in the NCBI Gene Expression Omnibus under accession number GEO: GSE98729.

A *Generation of Grin1$^{fl/fl}$ mouse*

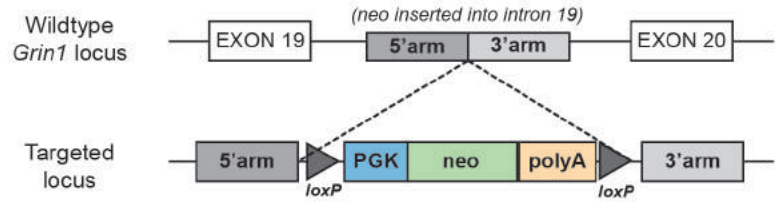

Biological mechanism of Grin1$^{fl/Cre}$ mouse model

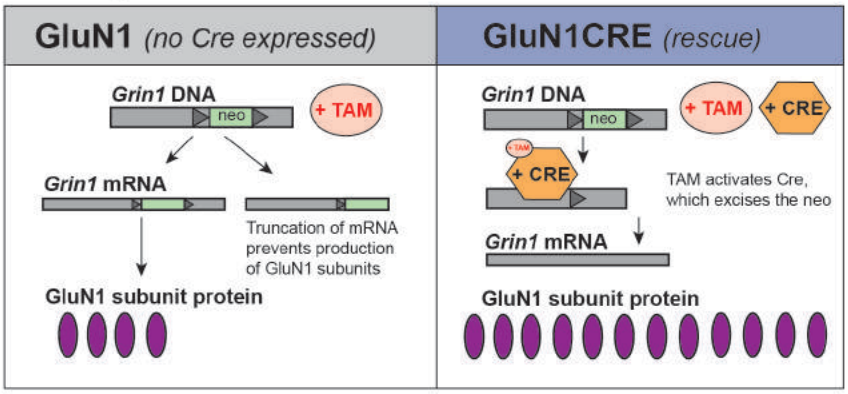

B *Global tamoxifen-induced Cre activity verified with tdTomato Cre reporter*

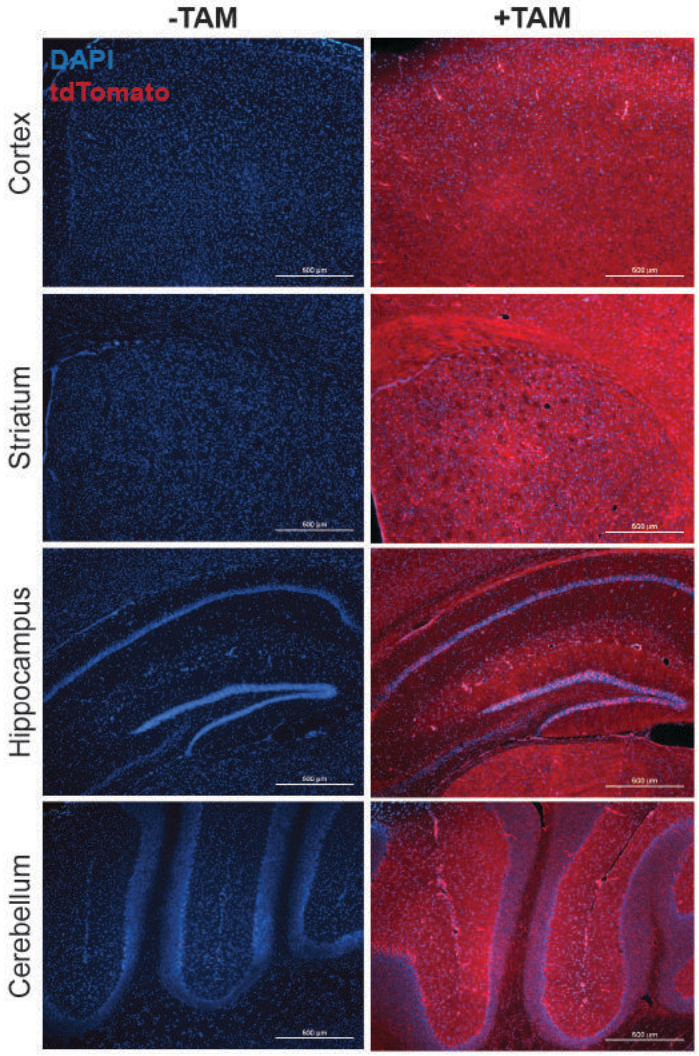

C *Rescue of GluN1 protein following tamoxifen administration*

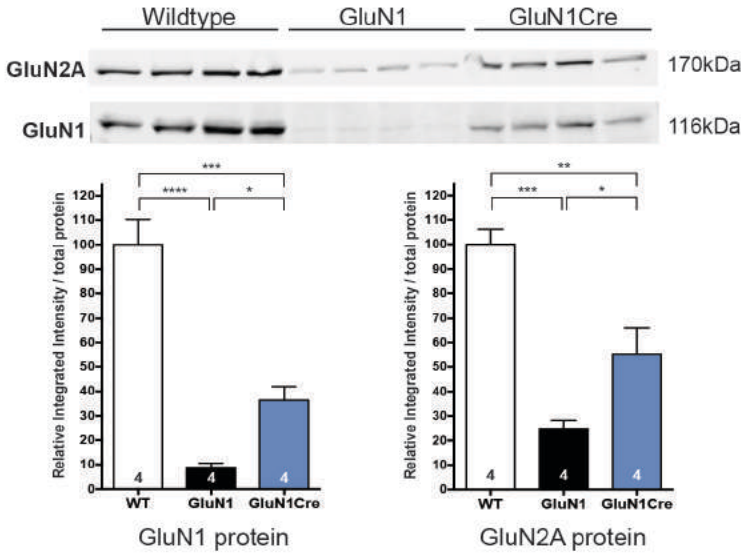

D *Tamoxifen intervention groups*

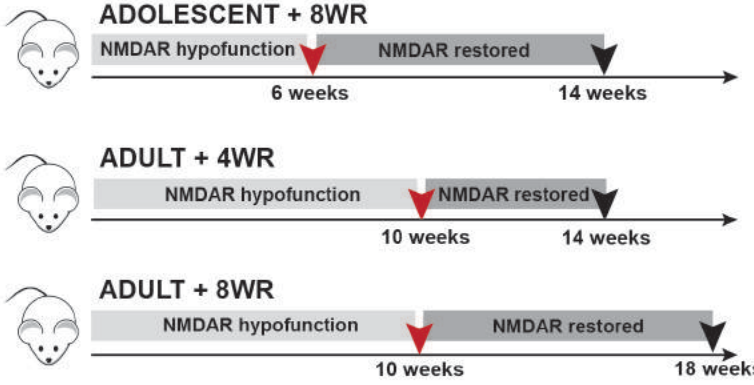

E *Timeline for behavioural testing*

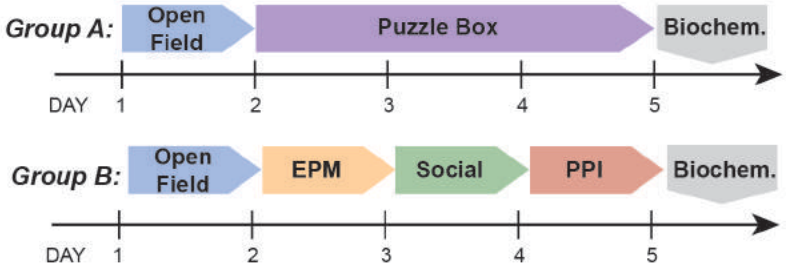

Table 1. **NMDA receptor binding densities of [^{3}H]MK-801 (fmol/mg) in brain tissue of WT, GluN1 and GluN1Cre mice.**

										Two – Way ANOVA					
	WT			**GluN1**			**GluN1Cre**			Genotype		Intervention Time		Genotype * Intervention	
Intervention Time Point	**Adol+8**	**Adult+4**	**Adult+8**	**Adol+8**	**Adult+4**	**Adult+8**	**Adol+8**	**Adult+4**	**Adult+8**	*F*(3,56)	*P*	*F*(2,56)	*P*	*F*(6,56)	*P*
Cortex	1756.0 ± 115.1	1531.0 ± 92.6	1679.0 ± 137.2	395.6 ± 41.7 22% WT	352.2 ± 20.9 23% WT	385.2 ± 34.0 23% WT	982.0 ± 58.2 56% WT	972.8 ± 60.6 63% WT	956.1 ± 75.4 57% WT	231.544	**<0.001**	20.594	0.231	49.814	0.559
Striatum	1030.0 ± 51.9	995.3 ± 55.5	904.4 ± 25.3	289.7 ± 10.9 28% WT	309.5 ± 14.6 31% WT	269.7 ± 18.9 30% WT	427.0 ± 15.1 41% WT	502.4 ± 40.5 50% WT	452.7 ± 44.4 50% WT	248.779	**<0.001**	0.624	0.539	0.923	0.485
Hippocampus	1698.0 ± 164.9	1868.0 ± 105.9	2051.0 ± 200.0	166.0 ± 31.2 10% WT	279.2 ± 28.9 15% WT	254.9 ± 29.8 12% WT	835.3 ± 48.9 49% WT	922.7 ± 48.2 49% WT	994.0 ± 77.5 48% WT	361.309	**<0.001**	3.712	**0.031**	2.017	0.079
Cerebellum	215.0 ± 21.6	224.0 ± 12.8	203.6 ± 11.8	85.4 ± 11.8 39% WT	72.3 ± 4.9 32% WT	63.1 ± 4.1 31% WT	105.3 ± 10.1 49% WT	109.2 ± 8.4 49% WT	119.7 ± 13.2 59% WT	118.853	**<0.001**	1.786	0.177	1.276	0.283

Data expressed as mean ± SEM in fmol/mg of protein. N=5-6/group, combined and equally balanced for sex. Multiple comparisons two-way ANOVA with Bonferroni's post-hoc.

RESCUED BEHAVIOURS - CORTICAL

A Executive Function

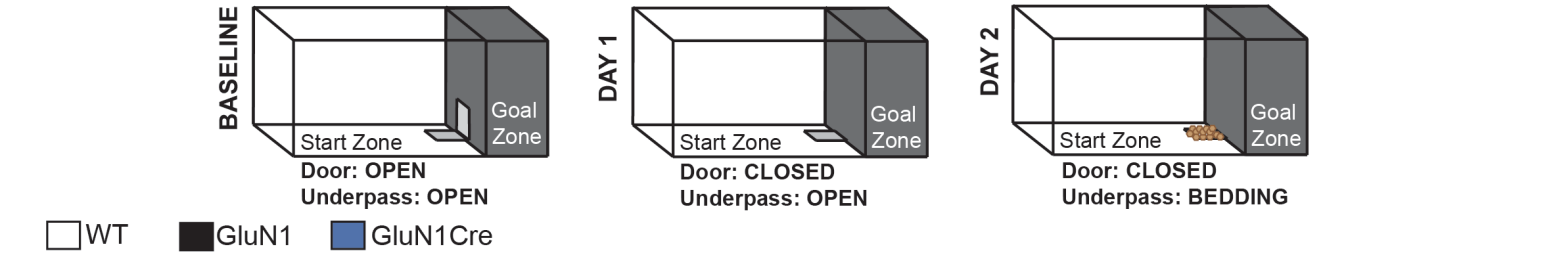

B Social Affiliative Behaviour

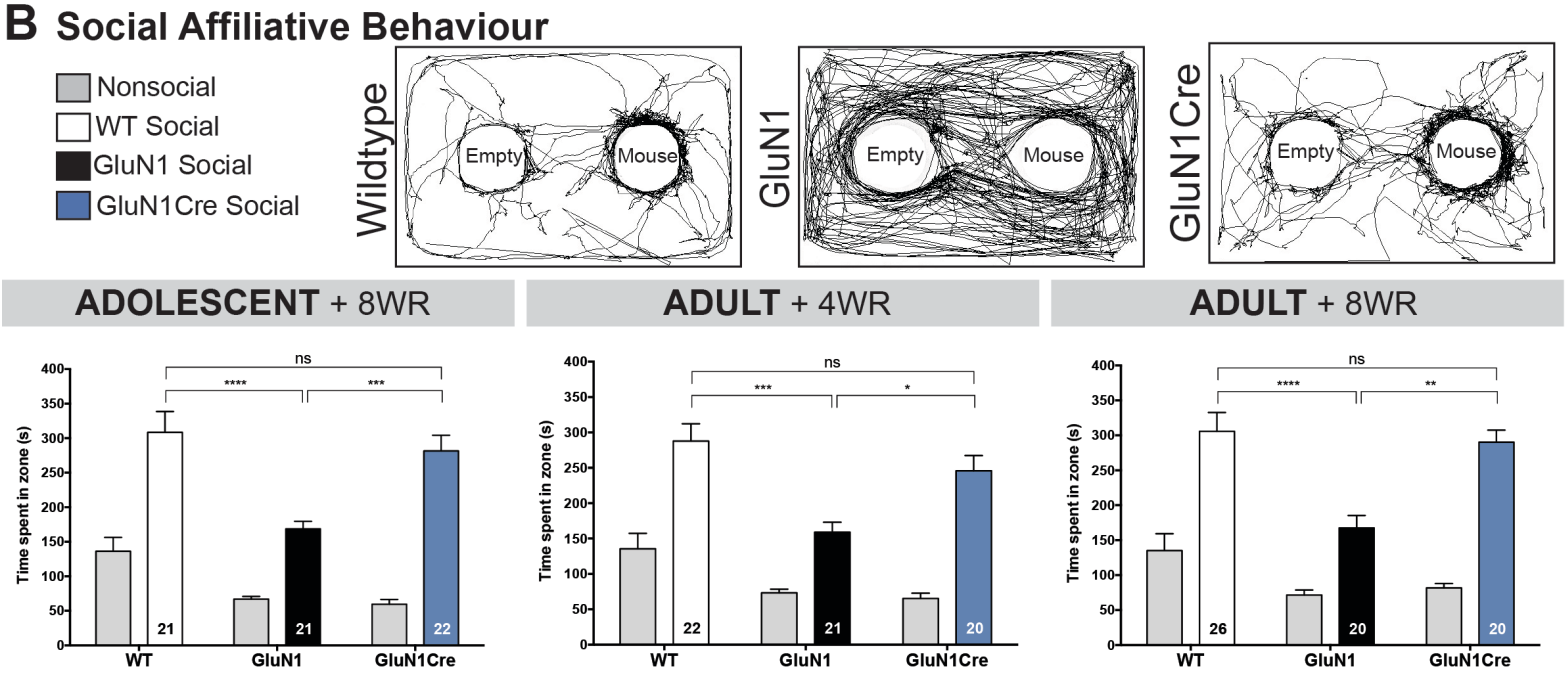

RESCUE-RESISTANT BEHAVIOURS - SUBCORTICAL

C Anxiety-Like Behaviour

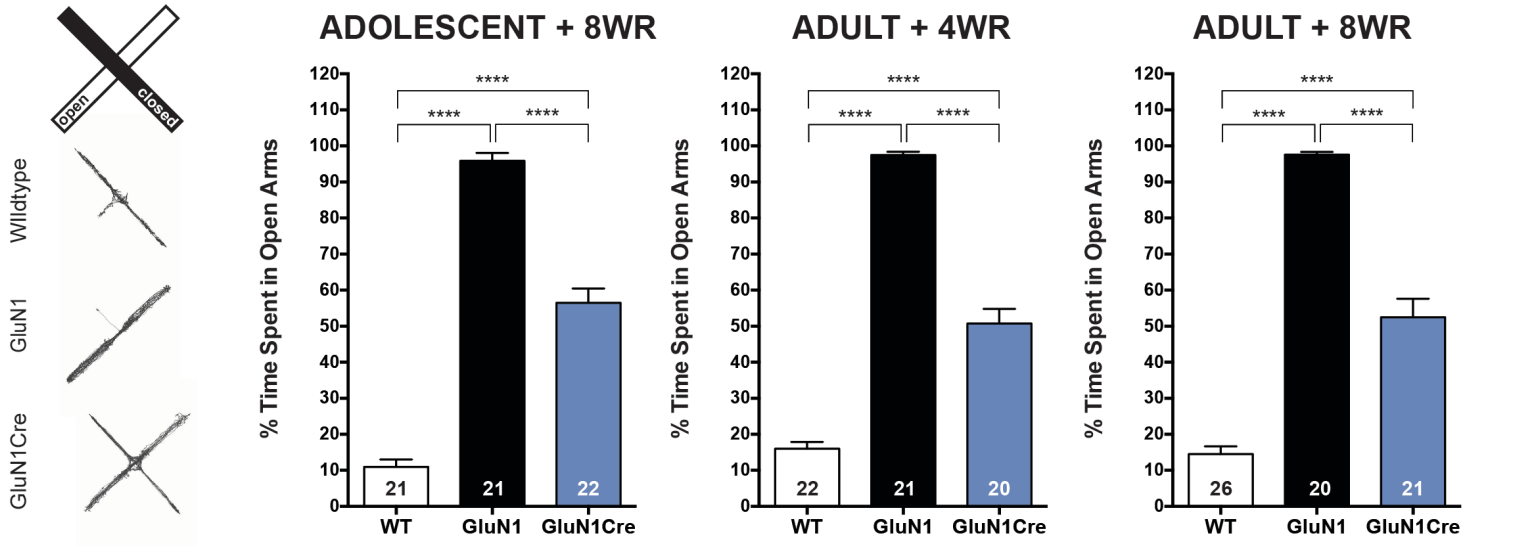

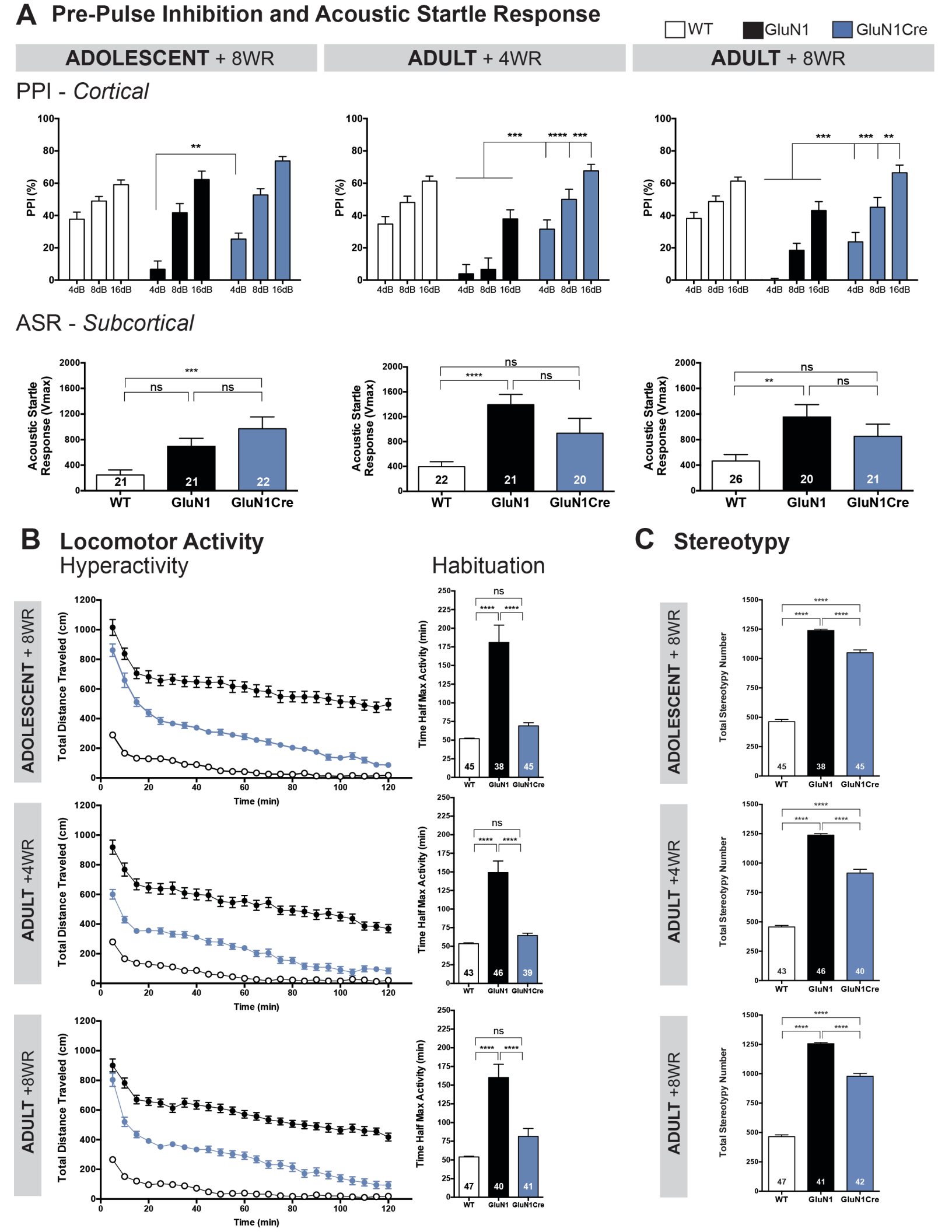
A Pre-Pulse Inhibition and Acoustic Startle Response
WT
GluN1
GluN1Cre
ADOLESCENT + 8WR
ADULT + 4WR
ADULT + 8WR
PPI - Cortical
PPI (%)
4dB 8dB 16dB
ASR - Subcortical
Acoustic Startle Response (Vmax)
ns
WT
GluN1
GluN1Cre
B Locomotor Activity
Hyperactivity
Habituation
Total Distance Traveled (cm)
Time (min)
Time Half Max Activity (min)
C Stereotypy
Total Stereotypy Number

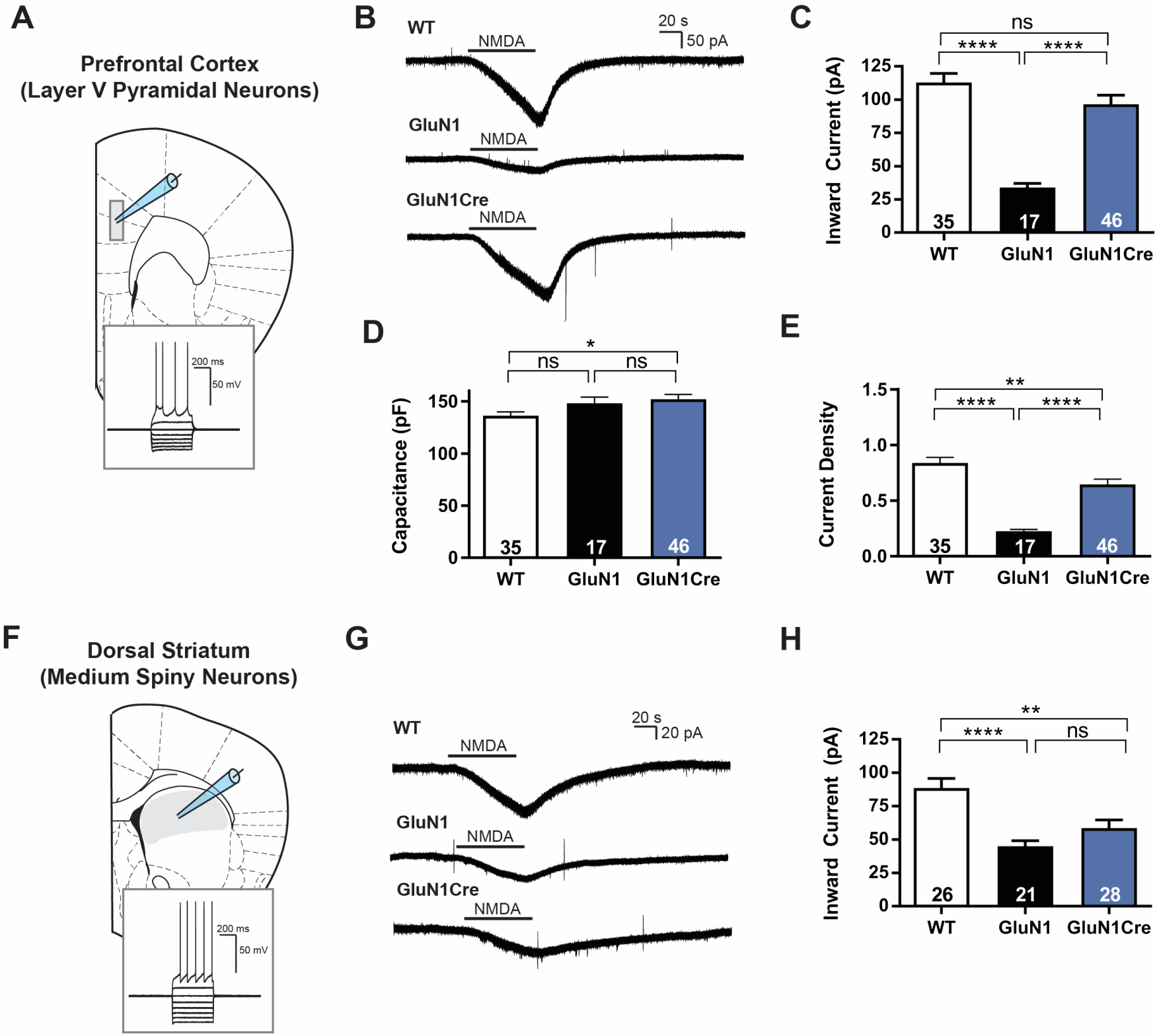
A
Prefrontal Cortex
(Layer V Pyramidal Neurons)
200 ms
50 mV
B
WT
NMDA
20 s
50 pA
GluN1
NMDA
GluN1Cre
NMDA
C
ns
****
****
Inward Current (pA)
125
100
75
50
25
0
35
17
46
WT
GluN1
GluN1Cre
D
*
ns
ns
Capacitance (pF)
150
100
50
0
35
17
46
WT
GluN1
GluN1Cre
E
**
****
****
Current Density
1.5
1.0
0.5
0.0
35
17
46
WT
GluN1
GluN1Cre
F
Dorsal Striatum
(Medium Spiny Neurons)
200 ms
50 mV
G
WT
NMDA
20 s
20 pA
GluN1
NMDA
GluN1Cre
NMDA
H
**
****
ns
Inward Current (pA)
125
100
75
50
25
0
26
21
28
WT
GluN1
GluN1Cre

A Gene expression in GluN1Cre mice

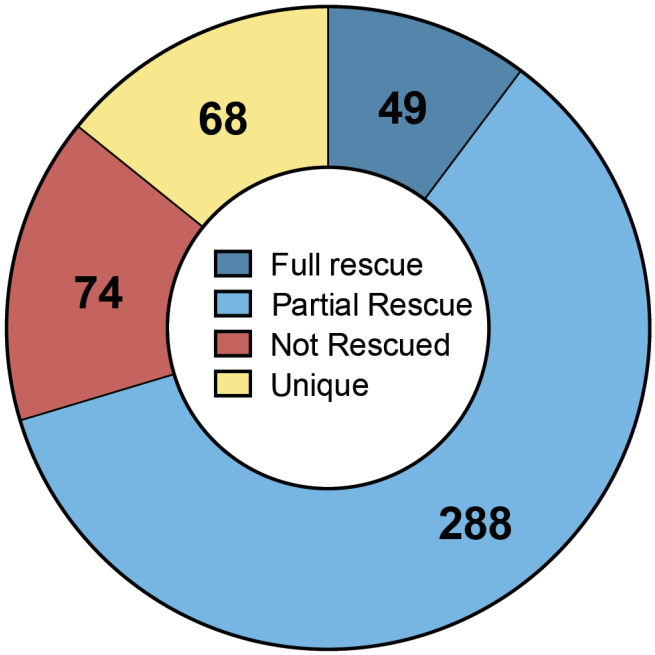

B Neurogenesis pathway

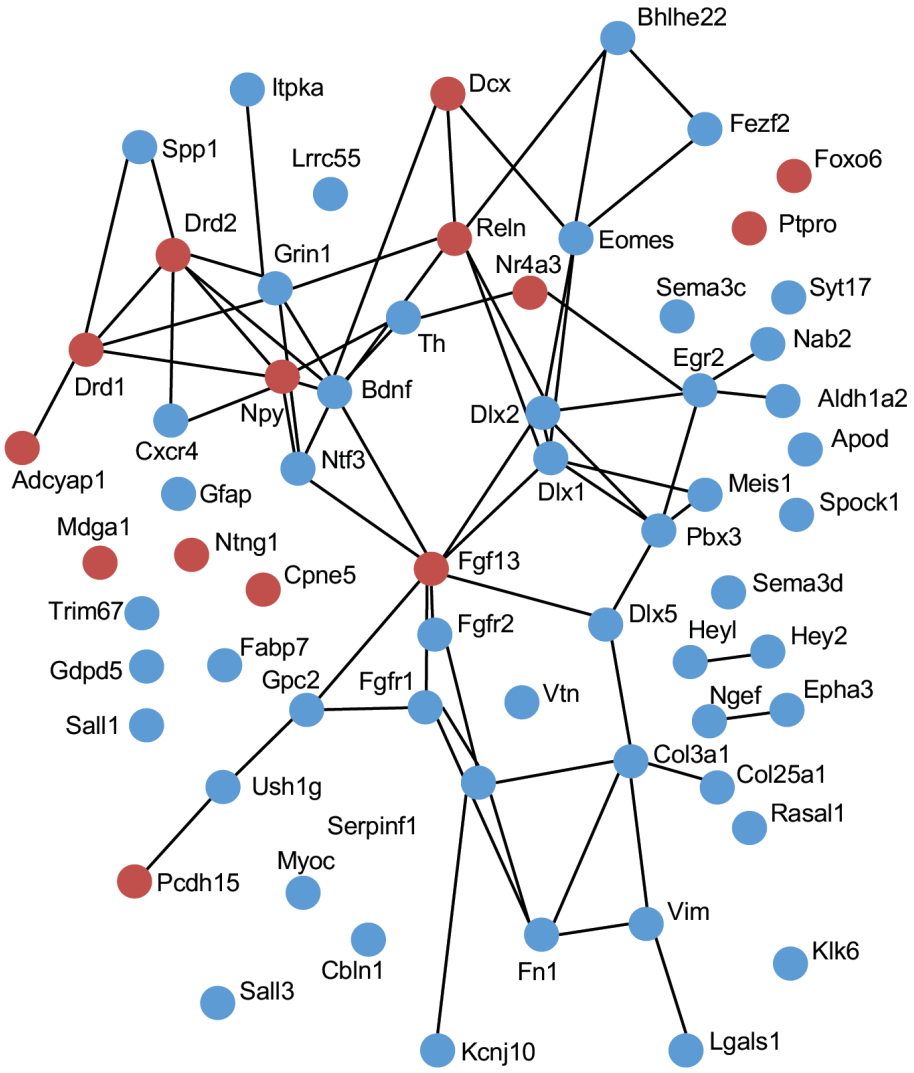

C Greatest changes of expression in GluN1 mice and its amelioration

	Log2 of fold change relative to WT	
	GluN1	GluN1Cre
Acan	1.222	0.989
Adamts19	1.405	0.862
Alpk3	1.068	0.523
Aqp1	1.431	0.855
Arhgef16	1.094	0.543
Calb2	1.349	0.644
Cbln1	1.062	0.518
Cdhr1	1.038	0.483
Chrnb4	1.774	1.117
Clca1	1.261	0.995
Cpa6	1.029	0.792
Crh	1.288	0.557
Dnahc11	1.379	1.054
Nudt8	1.148	0.455
Eomes	2.190	1.292
Fam19a3	1.739	1.091
Foxd3	2.040	1.142
Fst	1.193	0.972
Gdpd4	1.134	0.457
Gkn3	-1.178	-0.032
Gpr50	1.313	0.700
Grem1	1.131	0.694
Grin1	-1.285	-0.823
Kcnk15	2.010	0.840
Klhl30	2.721	1.667
Lgr5	1.207	0.775
Lgr6	1.292	0.754
Ltbp2	1.459	0.600
Ms4a15	1.968	1.100
Myoc	-1.371	-0.457
Npffr2	1.239	0.849
Ntf3	-1.093	-0.671
Olfr78	-1.068	-1.053
Otop2	1.147	0.654
Plb1	1.227	0.785
Ppm1j	1.679	1.082
Prss56	1.132	0.636
Rab37	1.309	0.699
Rmrp	2.706	0.638
Rpph1	2.565	0.226
S100a5	2.630	1.434
Scgn	1.956	1.373
Shisa3	2.297	1.330
Slc43a3	1.111	0.770
Slc9a4	1.327	0.351
Snhg7	-1.286	-1.534
Sp7	1.217	0.549
Stoml3	2.103	1.093
Tbx21	2.578	1.476
Tfap2c	1.883	0.908
Th	1.469	0.666
Trh	1.562	0.660
Trp73	1.002	0.264
Ucma	1.183	0.819
Ush1g	2.191	1.021
Vipr2	1.424	0.657

Table 2. **Significantly altered biological processes due to GluN1 knockdown and rescue.**

RESPONSIVE TO RESCUE

Biological Process	Representation of genes within set	p-value	q-value	Genes
Trans-Synaptic Signaling	34/607 (5.6%)	3.16E-10	1.53E-07	*Cbln1, Chrm2, Crh, Crhbp, Flot2, Gad1, Gad2, Gfap, Glra2, Gpr149, Grin1, Itpka, Itpr3, Jph4, Kcnj10, Kcnq3, Kcnq5, Kcnmb4, Ntf3, Slc6a9, Slc6a11, Slc6a13, Slc8a2, Slc22a2, Sst, Sstr1, Stx1a, Syt6, Syt10, Syt17, Sytl2, Th, Vgf, Unc13c*
Cation Transport	41/1054 (3.9%)	1.81E-07	2.91E-05	*Abcc8, Akap7, Aqp1, Atp2b4, Atp2c2, Cacna1s, Cacng5, Crh, Crhbp, Cxcr4, Grin1, Hcn4, Igf1, Itpr3, Jph4, Kcnab1, Kcnab3, Kcnh3, Kcnj10, Kcnk2, Kcnk15, Kcnmb4, Kcnq3, Kcnq5, Kcnv1, Nnt, Rapgef3, Slc6a9, Slc8a2, Slc9a2, Slc9a4, Slc13a3, Slc17a8, Slc22a2, Slc30a3, Slc38a3, Tcn2, Trdn, Ubash3b, Ucp2, Wnk4*
Response to Corticosteroid	15/182 (8.2%)	3.02E-07	3.66E-05	*Aqp1, Cdkn1a, Col1a1, Crh, Eln, Fn1, Hmgcs2, Igf1, Igfbp2, Lcat, Ptgds, Serpinf1, Sparc, Th, Trh*
Neurogenesis	49/1433 (3.4%)	4.97E-07	3.76E-05	*Aldh1a2, Apod, Bdnf, Bhlhe22, Cbln1, Col3a1, Col25a1, Cxcr4, Dlx1, Dlx2, Dlx5, Eomes, Epha3, Fabp7, Fgfr1, Fgfr2, Fn1, Fezf2, Gdpd5, Gfap, Gpc2, Grin1, Hey2, Heyl, Itpka, Kcnj10, Klk6, Lgals1, Lrrc55, Meis1, Myoc, Nab2, Ngef, Ntf3, Pbx3, Rasal1, Sall1, Sall3, Sema3c, Sema3d, Serpinf1, Spock1, Spp1, Syt17, Th, Trim67, Vim, Vtn, Ush1g*

RESISTANT TO RESCUE

Biological Process	Representation of genes within set	p-value	q-value	Genes
Trans-Synaptic Signaling	13/607 (2.1%)	1.20E-07	1.49E-05	*Adcyap1, Arc, Chrnb3, Chrnb4, Cplx2, Cplx3, Drd1, Drd2, Egr2, Otof, Npffr2, Npy, Reln*
Adenylate Cyclase Activity	6/71 (8.6%)	1.47E-07	1.49E-05	*Adcyap1, Adora2a, Drd1, Drd2, Hpca, Npffr2*
Neurogenesis	15/1433 (1.0%)	8.25E-05	0.00186	*Adcyap1, Cpne5, Dcx, Drd1, Drd2, Egr2, Fgf13, Foxo6, Mdga1, Ntng1, Npy, Nr4a3, Pcdh15, Ptpro, Reln*